Molecular Therapy
Original Article

Targeting tissue-resident memory CD8$^+$ T cells in the kidney is a potential therapeutic strategy to ameliorate podocyte injury and glomerulosclerosis

Liang Li,[1] Wei Tang,[2] Yan Zhang,[1] Meng Jia,[1] Limei Wang,[4] Quanxin Li,[1] Qingsheng Han,[1] Xiuping Peng,[1] Yusheng Xie,[1] Jichao Wu,[1] Ziying Wang,[1] Junhui Zhen,[3] Xiaojie Wang,[1] Min Liu,[1] Yu Sun,[1] Chun Zhang,[5] and Fan Yi[1]

[1]The Key Laboratory of Infection and Immunity of Shandong Province, Department of Pharmacology, School of Basic Medical Sciences, Shandong University, Jinan, Shandong 250012, China; [2]Department of Pathogenic Biology, School of Basic Medical Sciences, Shandong University, Jinan 250012, China; [3]Department of Pathology, School of Basic Medical Sciences, Shandong University, Jinan 250012, China; [4]Advanced Medical Research Institute, Cheeloo College of Medicine, Shandong University, Jinan 250012, China; [5]Department of Nephrology, Union Hospital, Tongji Medical College, Huazhong University of Science and Technology, Wuhan 430022, China

Although tissue-resident-memory T (T_{RM}) cells, a recently identified non-circulating memory T cell population, play a crucial role in mediating local immune responses and protect against pathogens upon local reinfection, the composition, effector function, and specificity of T_{RM} cells in the kidney and their relevance for chronic kidney disease remain unknown. In this study, we found that renal tissue displayed high abundance of tissue-resident lymphocytes, and the proportion of CD8$^+$ T_{RM} cells was significantly increased in the kidney from patients and mice with focal segmental glomerulosclerosis (FSGS), diabetic kidney disease (DKD), and lupus nephritis (LN). Mechanistically, IL-15 significantly promoted CD8$^+$ T_{RM} cell formation and activation, thereby promoting podocyte injury and glomerulosclerosis. Interestingly, Sparsentan, the dual angiotensin II (Ang II) receptor and endothelin type A receptor antagonist, can also reduce T_{RM} cell responses by intervening IL-15 signaling, exploring its new pharmacological functions. Mechanistically, Sparsentan inhibited Ang II or endothelin-1 (ET-1)-mediated IL-15 signaling, thereby further regulating renal CD8$^+$ T_{RM} cell fates. Collectively, our studies provide direct evidence for the pivotal role of renal CD8$^+$ T_{RM} cells in podocyte injury and further strengthen that targeting T_{RM} cells represents a novel therapeutic strategy for patients with glomerular diseases.

INTRODUCTION

Tissue-resident-memory T (T_{RM}) cells, a recently identified non-circulating memory T cell population mainly located in barrier tissues at interfaces with the environment, play a crucial role in mediating potent local immune responses and provide a long-term localized defense against pathogens.[1–3] The formation and maintenance of T_{RM} cell are influenced by numerous factors, including inflammation, antigen triggering, and tissue-specific cues.[4,5] Emerging evidence has revealed that T_{RM} cells are also present in the kidney and other non-barrier tissues.[6] Recent studies have found a marked increase in CD4$^+$ T_{RM} cells in kidney biopsies from patients with antineutrophil cytoplasmic antibody (ANCA)-dependent glomerulonephritis and further confirmed that infection-induced CD4$^+$ T_{RM} cells may rapidly react to local inflammatory cytokines and aggravate renal autoimmune diseases, supporting a new concept for the predisposing role of microbial infections in aggravating autoimmune diseases.[7] However, most studies so far mainly focus on T_{RM} cells and their relevance for immediate protection against pathogens upon local reinfection; the composition, localization, effector function, and specificity of T_{RM} cells in the kidney and their relevance for chronic kidney disease (CKD) remain unknown.

Podocytes are highly differentiated epithelial cells and are essential for the formation and maintenance of the glomerular filtration barrier.[8] Despite compelling evidence identifying podocyte injury as the key mediator in the pathogenesis of glomerular diseases, such as focal segmental glomerulosclerosis (FSGS), minimal change disease (MCD), diabetic kidney disease (DKD), and lupus nephritis (LN), the delivery of efficient therapies targeting podocytes is still a great challenge. On the other hand, podocyte injuries are closely associated with disruption of immune homeostasis.[9,10] Podocytes share many elements of the innate and adaptive immune system. They not only produce and express complement components and receptors but also express both class I and II major histocompatibility complex (MHC) molecules and co-stimulatory molecules that are involved in local immune responses. Recent studies have reported that antigen presentation by podocytes under inflammatory conditions plays an important role in activating T cell immune responses and facilitating

Received 17 January 2022; accepted 29 April 2022;
https://doi.org/10.1016/j.ymthe.2022.04.024.

Correspondence: Fan Yi, Ph.D., Department of Pharmacology, School of Basic Medical Sciences, Shandong University Jinan, Jinan, Shandong 250012, P.R. China.
E-mail: fanyi@sdu.edu.cn

immune-mediated glomerular disease development. Meanwhile, inflammatory cytokines produced by T cells, such as interferon-γ (IFN-γ), can also induce the expression of MHC-I, MHC-II, CD80, and CD86 on podocyte surface, which promotes podocyte present antigen and podocyte apoptosis.[10] Therefore, a comprehensive understanding of the local immune responses associated with the activation and functions of T_{RM} cells in the kidney and their relevance of podocyte injury is necessary for the development of tissue-resident, cell-based immunotherapies for glomerular diseases.

In this study, we found that renal tissue displayed high abundance of tissue-resident lymphocytes, and the proportion of $CD8^+$ T_{RM} cells was significantly increased in the kidney from patients and mice with glomerular diseases. Mechanistically, interleukin-15 (IL-15) significantly promoted $CD8^+$ T_{RM} cell formation and activation, thereby promoting podocyte injury and glomerulosclerosis. Interestingly, Sparsentan, the dual angiotensin II receptor and endothelin type A receptor antagonist, can also reduce T_{RM} cell responses by intervening IL-15 signaling, exploring its new pharmacological functions. Collectively, our studies suggest pharmacological targeting of IL-15-mediated $CD8^+$ T_{RM} cell formation and activation at multiple levels may provide a novel approach for the treatment of glomerular diseases.

RESULTS

The kidney displays high abundance of T_{RM} cells

We performed a 42-antibody panel for mass cytometry to build a composite of human (Figures 1A and S1A) and murine (Figures 1B and S1B) renal leukocytes in the steady state. The immune landscape indicated that T lymphocytes were enriched in the kidney. CD69 expression on T cells is indicative of a tissue-resident phenotype[11] and almost all of renal $CD69^+$ T cells exhibited memory cell phenotypes: $CD45RA^-$ $CCR7^-$ in human (Figure S1C) and $CD44^+$ in mouse (Figure S1D). Next, we examined whether these renal $CD69^+CD44^+$ T cells exhibited tissue-resident features in mouse. *In vivo* labeling assay showed that renal $CD69^+CD44^+$ T cells were protected from intravenous (i.v.) injection antibody labeling ($CD45^-$) and they were *bona fide* resident population (Figure 1C). Phenotypic analysis showed that renal $CD69^+CD44^+$ T cells highly expressed tissue homing chemokine receptor CXCR3 but lowly expressed lymph node homing receptor CD62L (Figure 1D). Furthermore, they produced more effector molecular IFN-γ and perforin than renal $CD69^-CD44^+$ T cells (Figure 1E). Collectively, these data confirmed that the kidney harbored a large number of T_{RM} cells in human and mouse under homeostatic conditions.

The proportion of $CD8^+$ T_{RM} cells is significantly increased in mice and patients with glomerular diseases

We found that the proportion of $CD8^+$ T_{RM} cells was significantly increased in the kidney in independent mouse models for different glomerular diseases, including Adriamycin (ADR)-induced FSGS mice (Figure 2A), *db/db* mice (30 weeks of age, a spontaneous type 2 diabetes mellitus model, Figure 2B), and MRL/*lpr* mice (a mouse model of systemic lupus erythematosus, Figure 2C).[12] Among these animal models, the number of $CD8^+$ T_{RM} cells had no significant difference. Meanwhile, the proportion of $CD4^+$ T_{RM} cells in MRL/*lpr* mice was also increased (Figure S2C), but there were no changes in mice with ADR treatment and *db/db* mice compared with their normal controls (Figures S2A and S2B). We further measured cytokine production in isolated renal $CD8^+$ T_{RM} cells from mice under these pathological conditions and found that $CD8^+$ T_{RM} cells expressed more IFN-γ and perforin (Figures 2D–2F), indicating that T_{RM} cells were activated.

Importantly, immunofluorescent (IF) results showed that the number of $CD8^+$ T_{RM} cells was increased in the tubulointerstitium surrounding the glomeruli in renal biopsies from patients with FSGS, DKD, and LN (Figure 2G). The number of $CD4^+$ T_{RM} cells in renal biopsies from patients with LN was also increased, but there were no changes from patients with FSGS and DKD compared with healthy controls (Figure S2D). Together, our results indicate that $CD8^+$ T_{RM} cells may play a universal role in different glomerular diseases.

The increased $CD8^+$ T_{RM} cells are derived from peripheric $CD69^-$ memory T cells

To identify whether renal T_{RM} cells are derived from circulating $CD69^-$ memory T cells or the local proliferation of T_{RM} cells under pathological conditions, FTY720, a sphingosine-1-phosphate (S1P) inhibitor that prevents lymphocyte circulation,[13] was used for the pretreatment of mice (Figure 3A). There were no more proliferating renal T_{RM} cells in mice with ADR treatment (Figures 3B and 3C). Next, we further determined whether peripheric $CD69^-$ memory T cells differentiated into T_{RM} cells. We sorted $CD8^+CD69^-CD44^+$ T cells from normal mice and then transfused them to normal or ADR-treated nude mice (Figure 3D). Peripheral-infiltrating $CD8^+$ T cells were phenotyped by flow cytometry after 6 weeks of ADR treatment. It was found that more $CD69^+$ T cells were present in the kidney from ADR-treated transfused nude mice (Figure 3E) and highly expressed T_{RM} cells markers, such as CXCR3, and lowly expressed CD62L (Figure 3F). Therefore, we concluded that $CD8^+$ T_{RM} cells are derived from peripheral-infiltrating $CD69^-$ memory T cells under pathological conditions.

IL-15 promotes $CD8^+$ T_{RM} cell formation and activation in the kidney

We found that the level of IL-15 in the kidney was significantly increased in ADR-treated mice (Figure 4A) and positively correlated with the urine-albumin-to-creatinine ratio (UACR, Figure 4B). We further investigated whether IL-15 also regulates $CD8^+$ T_{RM} cell formation and activation as reported.[14] We isolated splenic mononuclear cells and sequential exposure to recombinant IL-15 (rIL-15). It was found that rIL-15 induced $CD69^+$ T cell development. As a negative control, IL-2, one cytokine that shares the β-chain with the receptor for IL-15[15] had no effects on CD69 expression (Figure 4C). Furthermore, IL-15 could directly promote IFN-γ production in $CD8^+$ T_{RM} cells (Figure 4D), indicating that IL-15 can activate renal $CD8^+$ T_{RM} cells.

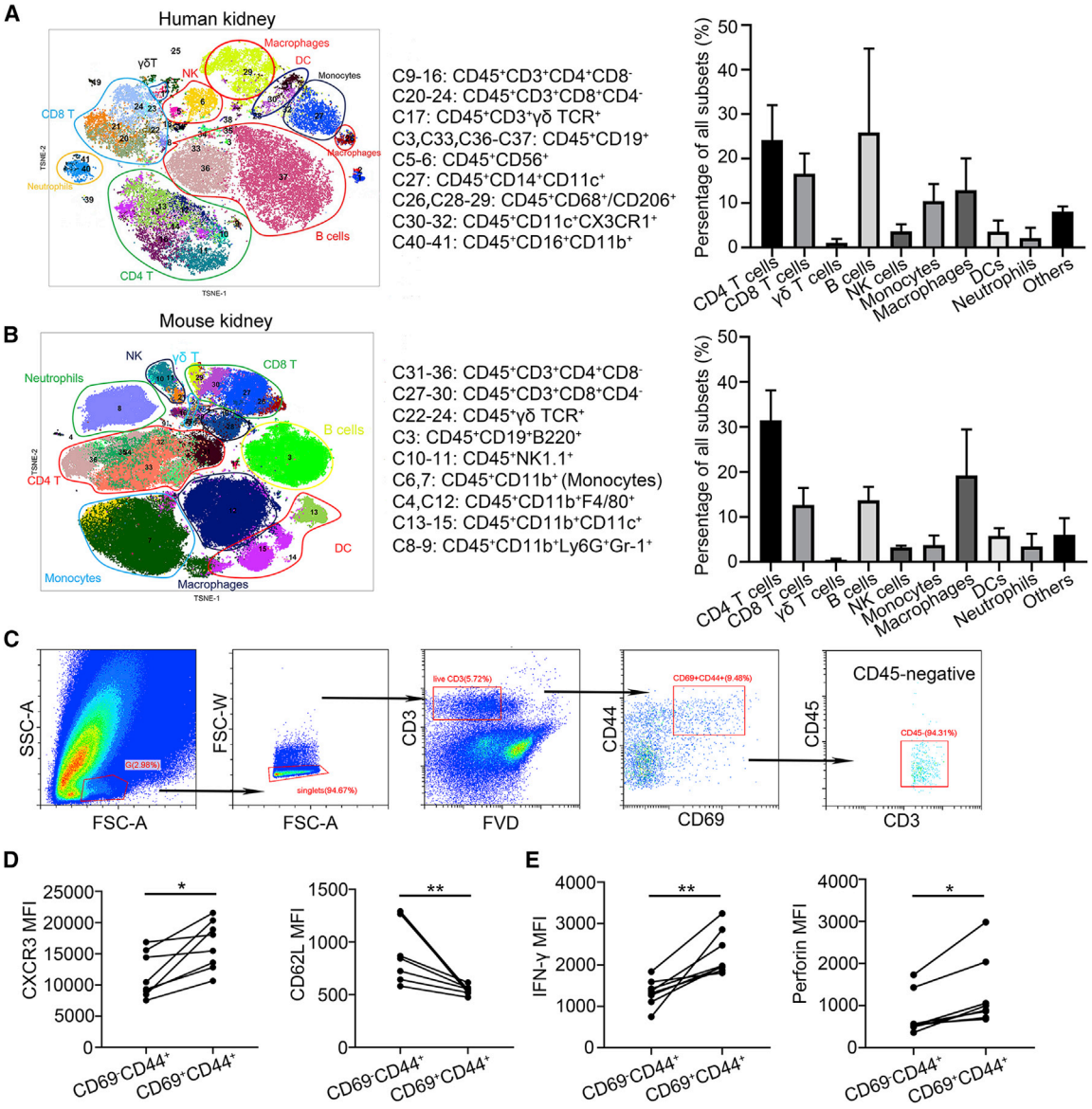

Figure 1. The kidney displays high abundance of T_{RM} cells

See also Figure S1. (A) Unsupervised cell cluster detection and quantification by t-distributed stochastic neighbor embedding (TSNE) and cytometry by time-of-flight (CyTOF) cluster detection algorithm on renal CD45$^+$ cells from normal human kidneys (n = 6). (B) Unsupervised cell cluster detection and quantification by TSNE and CyTOF cluster detection algorithm on renal CD45$^+$ cells from normal mouse kidneys (n = 6). (C) Gating strategy for renal intravascular staining after intravenous (i.v.) injection of allophycocyanin (APC) conjugated CD45 antibody. (D) The median fluorescence intensity (MFI) of CXCR3 and CD62L in renal CD69$^-$CD44$^+$ and CD69$^+$CD44$^+$ T cells individually (n = 8). (E) The MFI of IFN-γ and perforin in renal CD69$^-$CD44$^+$ and CD69$^+$CD44$^+$ T cells individually (n = 8). Data are represented as mean ± SEM. *p < 0.05, **p < 0.01.

IL-15 signaling blockade alleviates podocyte injury and glomerulosclerosis by inhibiting renal CD8$^+$ T_{RM} cell formation and activation

Considering that CD122 is an integral part of the receptor complex for IL-15,[16] CD122 was highly expressed in renal CD8$^+$ T_{RM} cells (Figure S3A), and anti-CD122 antibody inhibited IL-15-induced CD8$^+$ T_{RM} cell formation and activation *in vitro* (Figure S3B), we therefore injected anti-IL-15 or anti-CD122 antibody to ADR-treated nude mice, which were transfused CD8$^+$CD69$^-$CD44$^+$ T cells (Figure 4E). Anti-IL-15 or anti-CD122-antibody treatment significantly inhibited renal CD8$^+$ T_{RM} cell formation (Figure 4F) and activation (Figure 4G). Moreover, anti-IL-15- or anti-CD122-antibody-treated mice showed lower UACR (Figure 4H) and fewer glomerular and podocyte injuries (Figure 4I) compared with their controls. In addition, IL-15 signaling blockade recovered the expressions of nephrin and podocin (Figure 4J).

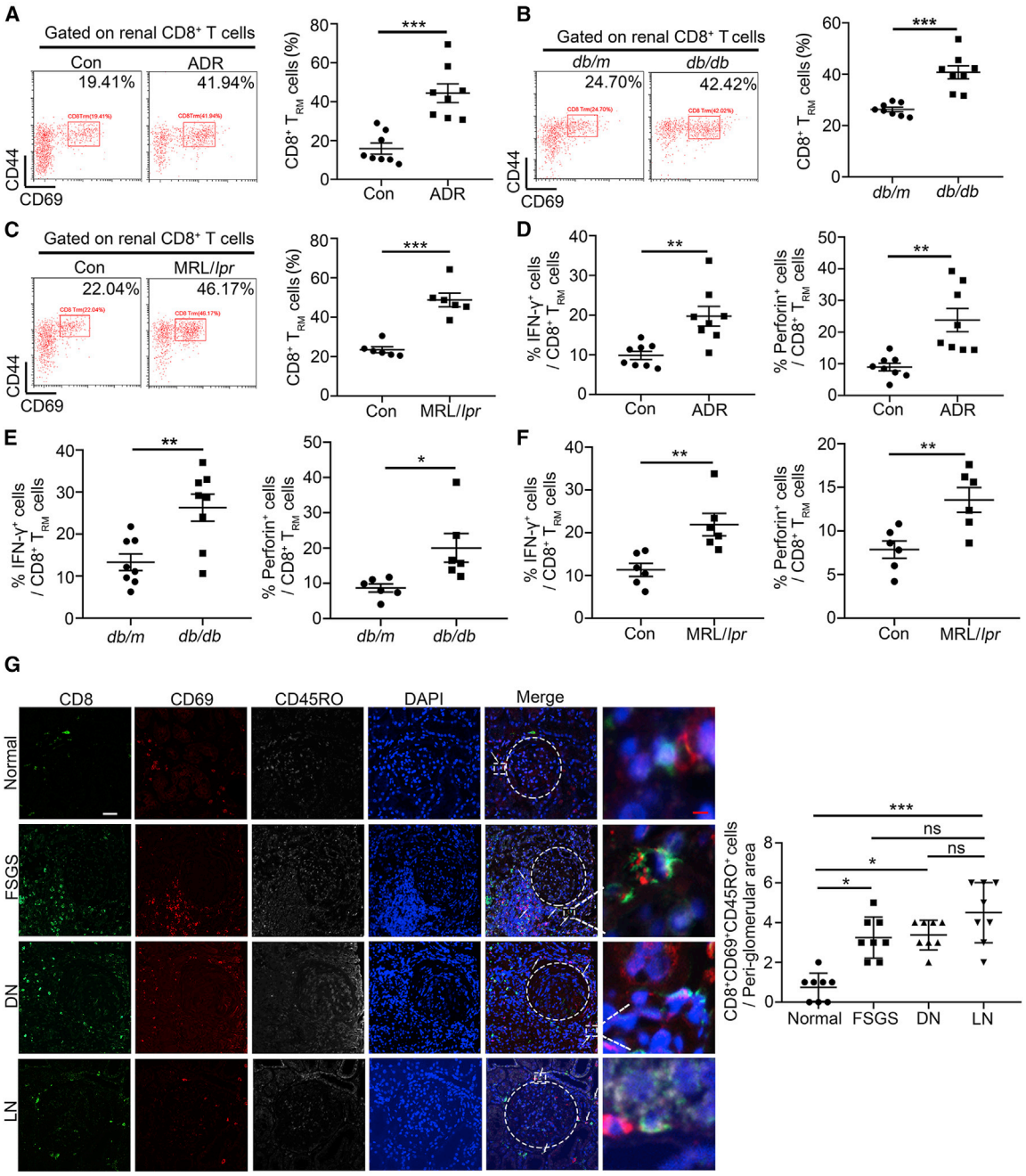

Figure 2. The proportion of CD8⁺ T_{RM} cells is significantly increased in mice and patients with glomerular diseases

See also Figure S2. (A–C) Representative flow cytometric analyses and quantification of renal CD8⁺ T_{RM} ($CD8^+CD69^+CD44^+$) cells in ADR-treated mice (A), *db/db* mice (B), MRL/*lpr* mice, (C) and their controls (n = 8). (D) The frequency of IFN-γ and perforin in renal CD8⁺ T_{RM} cells in control and ADR-treated mice (n = 8). (E) The frequency of IFN-γ (n = 8) and perforin (n = 6) in renal CD8⁺ T_{RM} cells in *db/m* and *db/db* mice. (F) The frequency of IFN-γ and perforin in renal CD8⁺ T_{RM} cells in control and MRL/*lpr* mice (n = 6). (G) Representative immunofluorescence staining for CD8 (green), CD69 (red), and CD45RO (gray) in human renal tissues from normal, subjects with FSGS diabetic nephropathy (DN) and LN. Left: representative images, white arrows highlight CD8⁺ T_{RM} cells ($CD8^+CD69^+CD45RO^+$); scale bars: white, 70 μm; red 5, μm; right: quantification of CD8⁺ T_{RM} cells surrounding the glomeruli per high power field (HPF, n = 8). Data are represented as mean ± SEM. *p < 0.05, **p < 0.01, ***p < 0.001, ns, no significance.

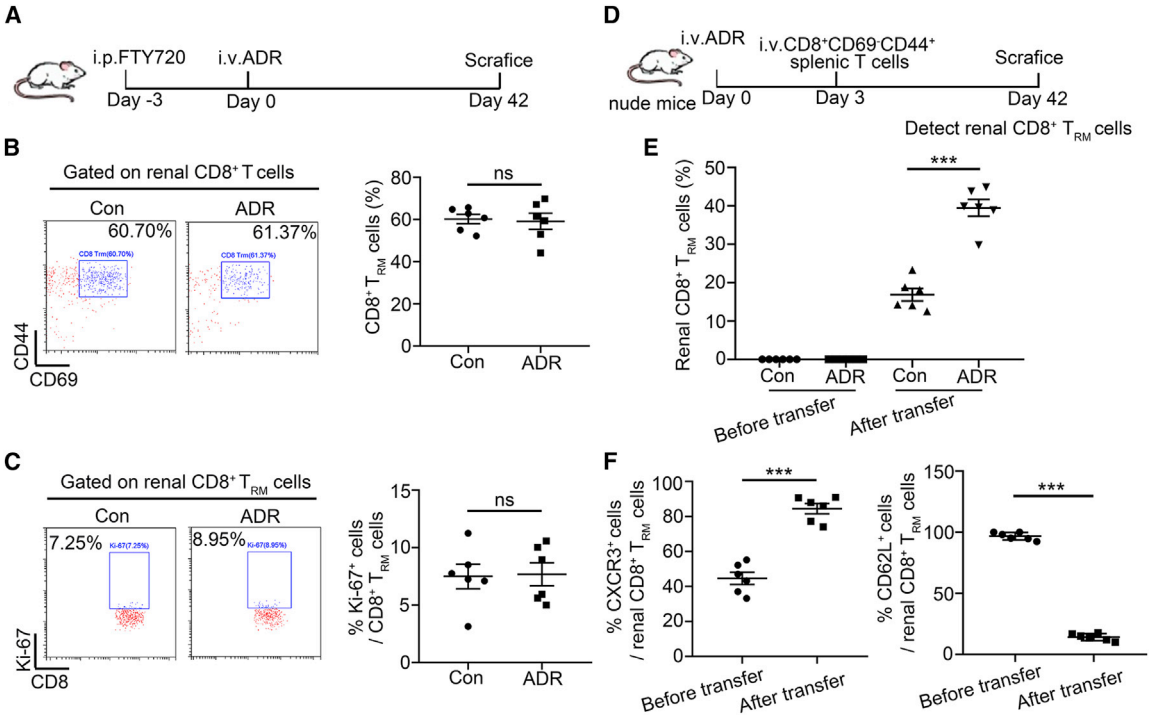

Figure 3. The increased CD8⁺ T_{RM} cells are derived from peripheric CD69⁻ memory T cells

(A) A schematic diagram showing the usage of FTY720 in ADR-treated mice. (B) Representative flow cytometric analyses and quantification of renal CD8⁺ T_{RM} cells (n = 6). (C) Representative flow cytometric analyses and the frequency of Ki-67⁺ cells in renal CD8⁺ T_{RM} cells (n = 6). (D) A schematic diagram showing that nude mice were adoptive transferred with splenic CD8⁺CD69⁻CD44⁺ T cells after ADR injection. Mice were euthanized at day 42. (E) The percentage of renal CD8⁺ T_{RM} cells from control or ADR-treated transfused nude mice (n = 6). (F) The percentage of CXCR3⁺ and CD62L⁺ cells in splenic CD8⁺CD69⁻CD44⁺ T cells (before transfer) and renal CD8⁺ T_{RM} cells (after transfer, n = 6). Data are represented as mean ± SEM. ***$p < 0.001$; ns, no significance.

Furthermore, in *db/db* mice, the level of IL-15 was also increased (Figure 4K) and positively correlated with the proteinuria (Figure 4L). Consistently, in anti-IL-15- or anti-CD122-antibody-treated *db/db* mice (Figure S4A), the formation and activation of renal CD8⁺ T_{RM} cell were markedly inhibited (Figures S4B and S4C). Lower urinary albumin excretion (Figure S4D) and less glomerulosclerosis and podocyte injury were also observed in *db/db* mice after anti-IL-15 or anti-CD122 antibody treatment (Figures S4E and S4F).

As a pleiotropic cytokine, IL-15 can also induce the proliferation of natural killer (NK) cells.[17] To investigate whether blocking of IL-15 signaling could affect NK cells and thereby alleviate podocyte and glomerular injuries, we injected *db/db* mice or ADR-induced mice with anti-NK1.1 antibody for three weeks and found that podocyte and glomerular injuries were not alleviated in mice with deficiency of NK cells, as shown in Figure S5, indicating that blocking of IL-15 signaling protects against podocyte and glomerular injuries, which may not be relevant to NK cells under these pathogenetic conditions.

Sparsentan inhibits CD8⁺ T_{RM} cell formation and activation

Sparsentan is a first-in-class, orally active, selective, and dual antagonist of the angiotensin II type 1 (AT_1) receptor and the endothelin type A (ET_A) receptor.[18,19] Interestingly, we occasionally found that Sparsentan (Figure 5A) could also reduce the number of renal CD8⁺ T_{RM} cells in mice with ADR treatment (Figure 5B). Moreover, Sparsentan reduced the production of IFN-γ (Figure 5C) and perforin (Figure 5D) in isolated renal CD8⁺ T_{RM} cells and alleviated proteinuria (Figure 5E), mesangial matrix expansion (Figure 5F), and podocyte injury (Figure 5G). To further confirm the broad implications of Sparsentan in conferring renal protection, we sought to investigate whether Sparsentan also has beneficial effects in *db/db* mice (Figure 5H). Consistently, Sparsentan inhibited CD8⁺ T_{RM} cell formation (Figure 5I) and activation (Figures 5J and 5K) and alleviated proteinuria (Figure 5L) and podocyte injury (Figures 5M–5N). These data provide direct evidence for the new pharmacological functions of Sparsentan. Targeting CD8⁺ T_{RM} cells may further strengthen therapeutic effects of Sparsentan besides directly acting on podocytes.

Angiotensin II and endothelin-1 induce IL-15 signaling

We found that the levels of angiotensin II (Ang II)[20] and endothelin-1 (ET-1) were enhanced in the kidney from mice with ADR treatment (Figure 6A) and *db/db* mice (Figure 6B), and the levels of Ang II (Figure 6C) and ET-1 (Figure 6D) were positively correlated with the level of IL-15. We further found that primary renal parenchymal cells secreted more IL-15 after Ang II or ET-1 treatment (Figure 6E). In addition, Sparsentan inhibited IL-15 production in the kidney from

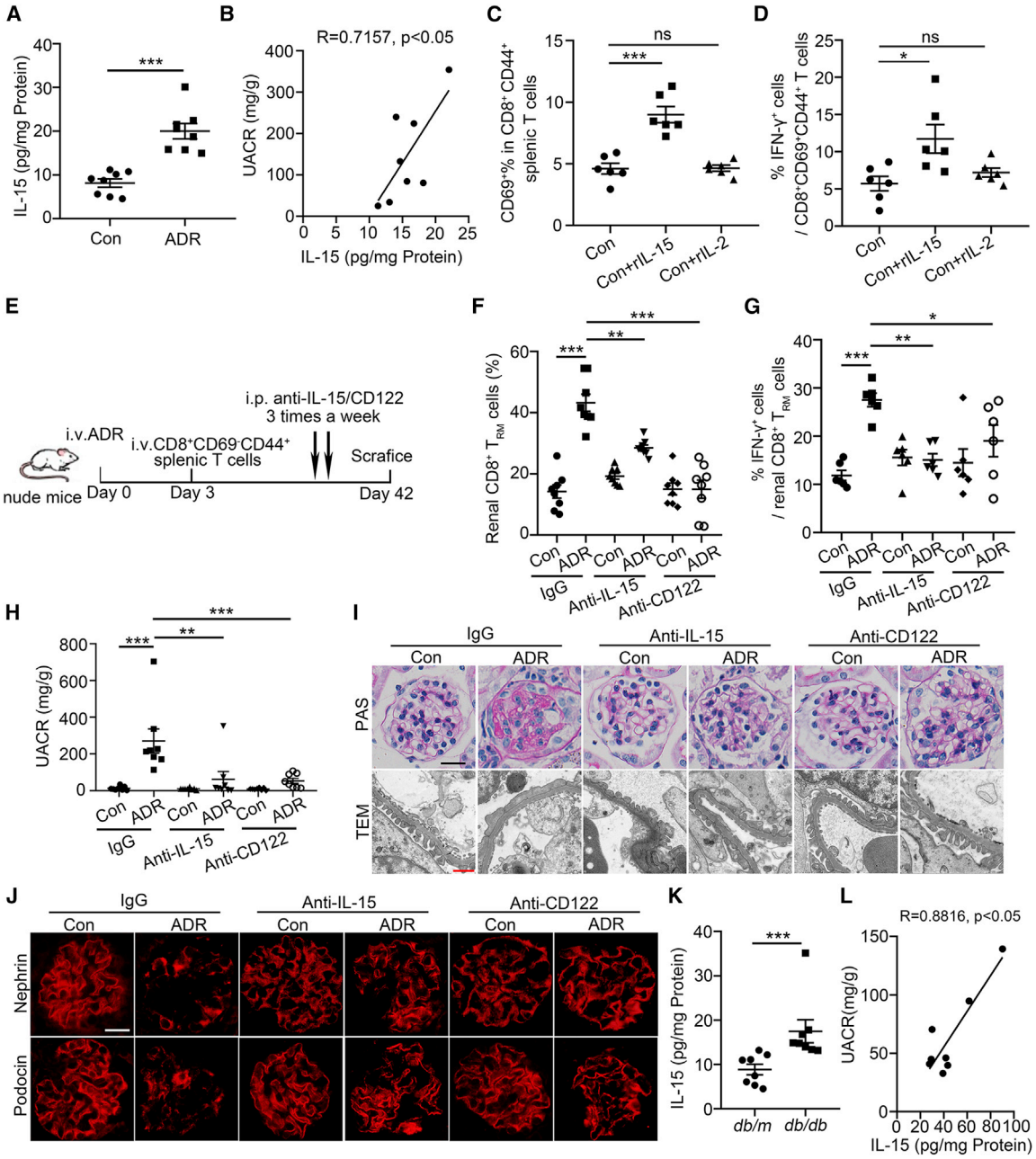

Figure 4. IL-15 signaling blockade alleviates glomerulosclerosis and podocyte injury by inhibiting renal CD8$^+$ T_{RM} cells formation and activation

See also Figures S3–S5. (A) The level of IL-15 in renal cortex of ADR-treated mice (n = 8). (B) Correlation between IL-15 and urine-albumin-to-creatinine ratio (UACR) in ADR-treated mice (n = 8). (C) The percentage of CD69$^+$ in splenic CD8$^+$CD44$^+$ T cells after 3-day culture in the presence of rIL-15 (50 ng/mL) or rIL-2 (50 ng/mL, n = 6). (D) The frequency of IFN-γ in splenic CD8$^+$CD69$^+$CD44$^+$ T cells after 3-day culture in the presence of rIL-15 (50 ng/mL) or rIL-2 (50 ng/mL, n = 6). (E) A schematic diagram showing anti-IL-15/CD122 treatment in transfused nude mice after ADR injection. (F) The percentage of renal CD8$^+$ T_{RM} cells in IgG- or anti-IL-15/CD122-treated control or ADR-treated transfused nude mice (n = 8). (G) The frequency of IFN-γ in renal CD8$^+$ T_{RM} cells from IgG- or anti-IL-15/CD122-treated control or ADR-treated transfused nude mice (n = 6). (H) UACR in mice (n = 8). (I) Morphological examinations of glomerular changes by periodic acid–Schiff (PAS) and transmission electron microscopy (TEM) analyses in mice. Scale bars: black, 20 μm; red, 1 μm. (J) Representative immunofluorescence images about nephrin and podocin expressions in glomeruli from mice. Scale bar, 20 μm. (K) The level of IL-15 in renal cortex of *db/db* mice (n = 8). (L) Correlation between IL-15 and UACR in *db/db* mice. R, Pearson correlation coefficient (n = 8). Data are represented as mean ± SEM. *p < 0.05, **p < 0.01, ***p < 0.001.

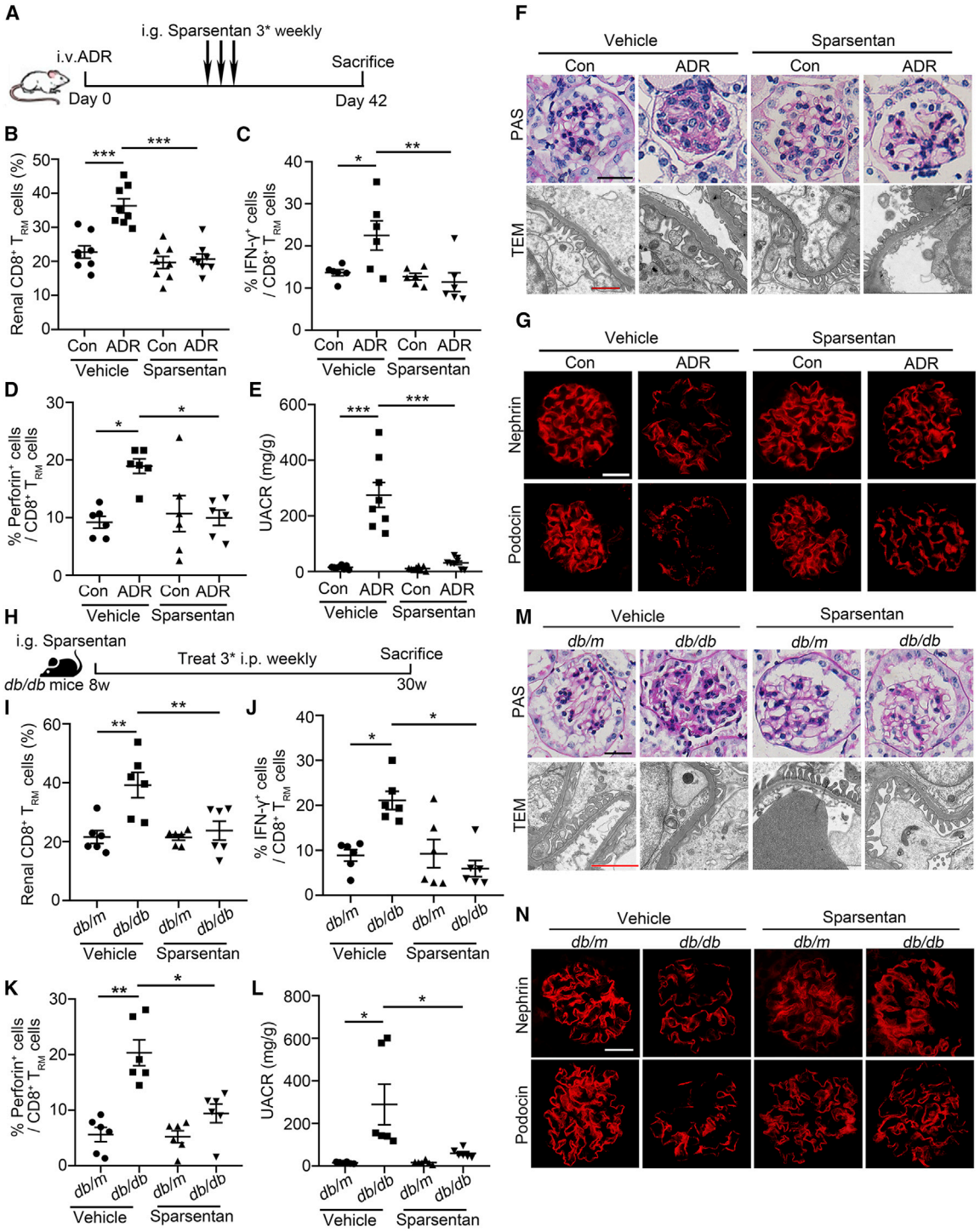

Figure 5. Sparsentan inhibits CD8$^+$ T_{RM} cell formation and activation and alleviates podocyte injury in ADR-treated mice and *db/db* mice

(A) A schematic diagram showing the treatment of Sparsentan in ADR-treated mice. (B) The percentage of renal CD8$^+$ T_{RM} cells in mice (n = 8). (C and D) The frequency of IFN-γ (C) and perforin (D) in renal CD8$^+$ T_{RM} cells (n = 6). (E) Urinary albumin-to-creatinine ratio (UACR) in mice (n = 8). (F) Morphological examinations of glomerular changes by periodic acid–Schiff (PAS) and transmission electron microscopy (TEM) analyses in mice. Scale bars: black 20, μm; red, 1 μm. (G) Representative immunofluorescence

(legend continued on next page)

mice with ADR treatment (Figure 6F) and *db/db* mice (Figure 6G). Our results suggest Sparsentan may inhibit IL-15 production, thereby further regulating renal $CD8^+$ T_{RM} cells fate under pathological conditions.

Activated renal $CD8^+$ T_{RM} cells trigger podocyte injury

To address the effects of renal $CD8^+$ T_{RM} cells on the regulation of podocyte function and fate,[10] we sorted renal $CD8^+CD69^-CD44^+$ T cells and $CD8^+$ T_{RM} cells from ADR-treated mice and then transferred them to normal nude mice. It was found that only $CD8^+$ T_{RM} cells triggered podocyte apoptosis (Figure 7A). *In vitro*, we isolated different types of renal memory T cells and co-cultured with murine podocytes. Similarly, only renal $CD8^+$ T_{RM} cells from ADR-treated mice had cytotoxic effects on podocytes, including enhanced apoptosis (Figure 7B), reduced nephrin and podocin expression (Figure 7C), induced actin cytoskeleton derangement, and mitochondria damage (Figure 7D). However, activated $CD8^+$ T_{RM} cells with pretreatment with anti-IL-15 or anti-CD122 antibody had less cytotoxicity (Figure 7E) and recovered the expressions of podocin in podocytes (Figure 7F). To evaluate the effects of $CD8^+$ T_{RM} cells on other renal parenchymal cells, we then co-cultured the activated renal $CD8^+$ T_{RM} cells and glomerular cells, such as mesangial cells or glomerular endothelial cells. It was found that $CD8^+$ T_{RM} cells had no significant effect on the fates of mesangial cells and endothelial cells (Figure S6). Consistently, Sparsentan alleviated podocyte injury, as evidenced by reduced apoptosis (Figure 7G), recovered podocin expression (Figure 7H), attenuated cytoskeleton, and mitochondria injury (Figure 7I), when we sorted renal $CD8^+$ T_{RM} cells from Sparsentan-treated ADR-treated mice and co-cultured with podocytes.

DISCUSSION

Podocyte dysfunction is central to the underlying pathophysiology of many common glomerular diseases, including DKD, FSGS, LN, and genetic forms of nephrotic syndrome.[8] By detection of immune landscape of human and mice kidney, we found that tissue-resident lymphocytes were present in the kidney. Although the function of renal T_{RM} cells under physiological conditions is still not very clear, previous studies have proposed that T_{RM} cells could be the consequence of a subclinical renal inflammation or infection. Renal T_{RM} cells might be involved in control of urogenital bacterial infection ascending to the kidney. It is also possible that T_{RM} cells are required to control latent chronic infections (e.g., by polyoma viruses).[21] More importantly, under pathogenetic conditions, the proportion of $CD8^+$ T_{RM} cells was substantially increased in the kidney from patients with glomerular diseases, such as FSGS, DKD, and LN, compared with healthy controls, as well as the kidney from experimental mouse models for these glomerular diseases. Meanwhile, we found that the number of $CD4^+$ T_{RM} cells was also increased in the kidney from mice and patients with LN, but not in FSGS and DKD, reflecting that $CD8^+$ T_{RM} cells but not $CD4^+$ T_{RM} cells may be a key and universal regulator contributing to glomerular injury. Therefore, considering that $CD8^+$ T_{RM} cells are undoubtedly attractive therapeutic targets with their distinct functions,[22–24] we further explored their regulatory mechanisms in glomerular diseases, including FSGS and DKD.

In this study, we demonstrated for the first time that $CD8^+$ T_{RM} cells in the kidney were mainly derived from $CD69^-$ memory T cells and further explored a previously unappreciated role of renal $CD8^+$ T_{RM} cells in podocyte injury through their cytotoxic effects on podocytes. The principal hallmark of *bona fide* $CD8^+$ T_{RM} cells is their long-term persistence in non-lymphoid tissues without recirculation in the blood. Differentiation of T_{RM} is controlled by various factors.[25] Our data support that targeting IL-15 signaling pathways is a potential strategy to clear autoreactive memory cells from the kidney and protects against podocyte injury in mice. Mechanistically, IL-15 promoted $CD8^+$ T_{RM} cell formation and activation. IL-15 is a pluripotent cytokine from the IL-2 family that possesses many functions involved in regulating both adaptive and innate immune systems. IL-15 has been investigated for its therapeutic potential for the induction and maintenance of T cell responses because of its unique properties, such as wide expression, tightly regulated secretion, and trans-presentation.[26] Studies have demonstrated that IL-15 is important for the generation of T_{RM} in viral infections and in cutaneous lymphomas,[27] and targeting IL-15 provides a durable treatment strategy for vitiligo.[16] In this study, we found that IL-15 was highly expressed in the kidney and was required for the formation and activation of $CD8^+$ T_{RM} cell under pathological conditions. Furthermore, we demonstrated that blocking of IL-15 signaling alleviated podocyte and glomerular injuries by inhibiting renal $CD8^+$ T_{RM} cells rather than NK cells, which was consistent with previous studies showing that NK cells cannot mediate renal injury in mice with ADR nephropathy.[28] Therefore, we suggest that inhibiting renal $CD8^+$ T_{RM} cells by targeting IL-15 signaling may provide a novel and durable treatment strategy for glomerular diseases.

In this study, another important finding is that Sparsentan can reduce T_{RM} cell responses by intervening IL-15 signaling, exploring its new pharmacological functions. In FSGS, current treatment with corticosteroids or other immunosuppressive drugs is aimed at reducing proteinuria.[29] These agents are routinely combined with renin-angiotensin system (RAS) inhibitors. Due to a spectrum of serious side effects of immunomodulating drugs, the availability of effective, safe, and well-tolerated drugs to protect renal function and reduce proteinuria is an unmet medical need in FSGS. Compared with RAS inhibitors, ET_A receptor antagonists have shown a wide range of beneficial hemodynamic, anti-inflammatory, anti-fibrotic, and podocyte-protective effects in glomerular diseases.[30,31] In particular, the combination of RAS inhibitors and ET_A receptor antagonists has additional benefits in experimental models of kidney diseases and in

images about nephrin and podocin expressions in glomeruli from mice. Scale bar, 20 μm. (H) A schematic diagram showing the treatment of Sparsentan in *db/db* mice. (I) The percentage of renal $CD8^+$ T_{RM} cells in mice (n = 6). (J and K) The frequency of IFN-γ (J) and perforin (K) in renal $CD8^+$ T_{RM} cells (n = 6). (L) UACR in mice (n = 6). (M) Morphological examinations of glomerular changes by PAS and TEM analyses in mice. Scale bars: black, 20 μm; red, 1 μm. (N) Representative immunofluorescence images about nephrin and podocin expressions in glomeruli from mice. Scale bar, 20 μm. Data are represented as mean ± SEM. *$p < 0.05$, **$p < 0.01$, ***$p < 0.001$.

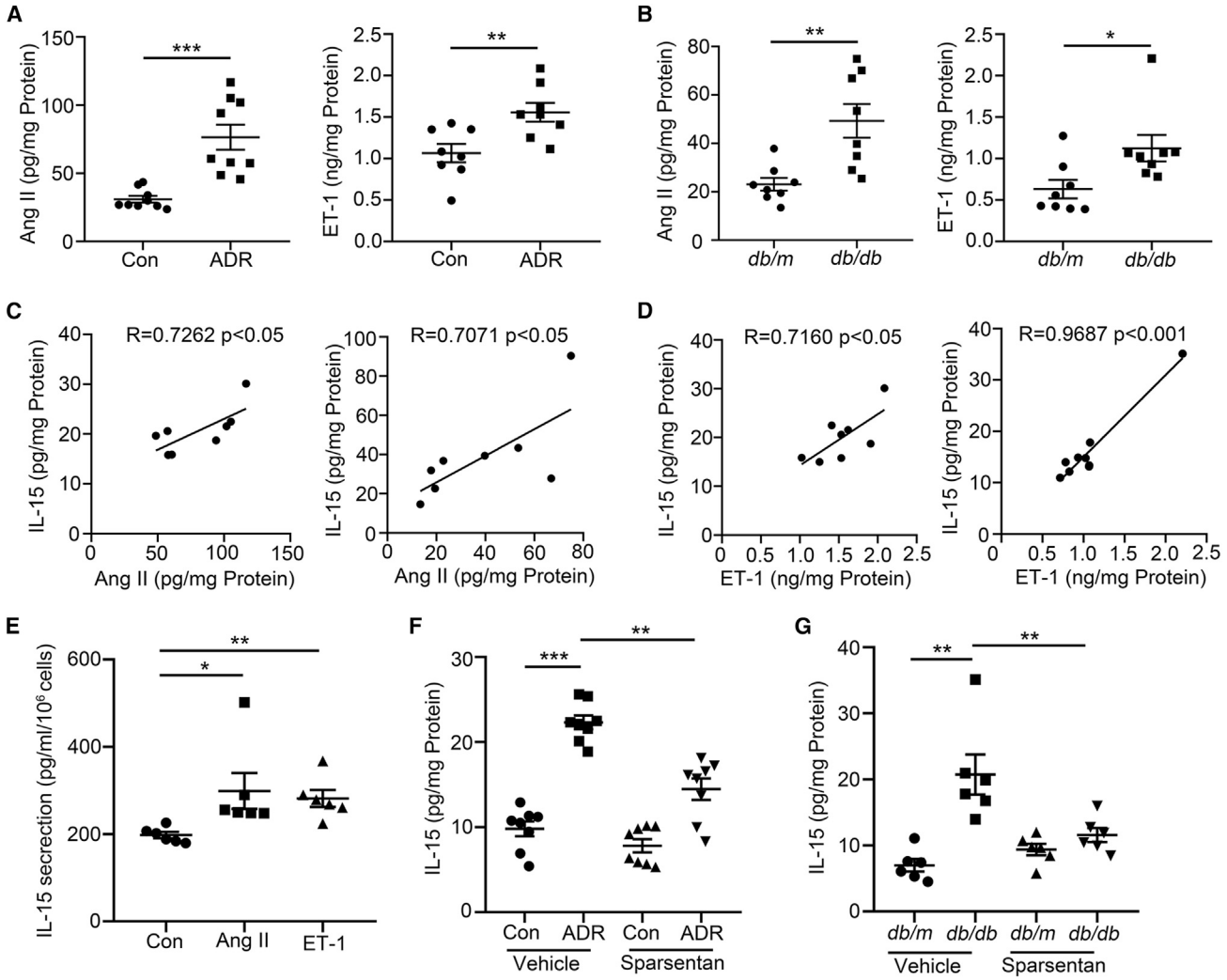

Figure 6. Angiotensin II and endothelin-1 induce IL-15 signaling

(A and B) The levels of angiotensin II (Ang II) and endothelin-1 (ET-1) in the renal cortex from ADR-treated mice (A, n = 9) and *db/db* mice (B, n = 8).

(C) Correlation between Ang II and IL-15 in renal cortex of ADR-treated and *db/db* mice (n = 8). R, Pearson correlation coefficient. (D) Correlation between ET-1 and IL-15 in renal cortex of ADR-treated and *db/db* mice (n = 8). R, Pearson correlation coefficient. (E) The secretion of IL-15 in primary renal parenchymal cells after Ang II (10^{-6} mol/L) or ET-1 (10^{-6} mol/L) treatment (n = 6).

(F and G) The level of IL-15 in renal cortex of ADR-treated mice (F, n = 8) and *db/db* mice (G, n = 6). Data are represented as mean ± SEM. *p < 0.05, **p < 0.01, ***p < 0.001.

patients with CKD.[32] Sparsentan is a first-in-class, orally active, selective, and dual antagonist of the AT_1 receptor and the ET_A receptor. Since 2020, a multicenter, international, phase 3, randomized, double-blind, active-controlled study of sparsentan in patients with FSGS (DUPLEX; NCT0349368528) trial has been initiated to evaluate the long-term nephroprotective effects and safety of Sparsentan in patients with primary FSGS.[33] In this study, we found that the levels of ET-1 and Ang II were significantly elevated and positively correlated with the level of IL-15 in the kidney from mice with FSGS or DKD. We further explored an unexpected role that Sparsentan can improve podocyte injury by inhibiting IL-15-mediated $CD8^+$ T_{RM} cell formation and activation, despite that we cannot exclude that Sparsentan may directly act on podocytes because Ang II and ET-1 have direct effect on podocyte function. Therefore, we propose that $CD8^+T_{RM}$-cell-dependent or -independent mechanisms may synergize together to protect against podocyte injury by Sparsentan. On the other hand, a feedforward mechanism may exist because the reduced proteinuria in glomerular diseases by Sparsentan may further decrease the $CD8^+$ T_{RM} cell formation and activation by the reduction of renal toxic local antigen.[34,35] Further studies are needed to address this issue.

Although in this study we demonstrate a contribution of $CD8^+$ T_{RM} cells to podocyte injury, further studies are required to elucidate why podocytes are more susceptible to the pathogenicity of renal $CD8^+$

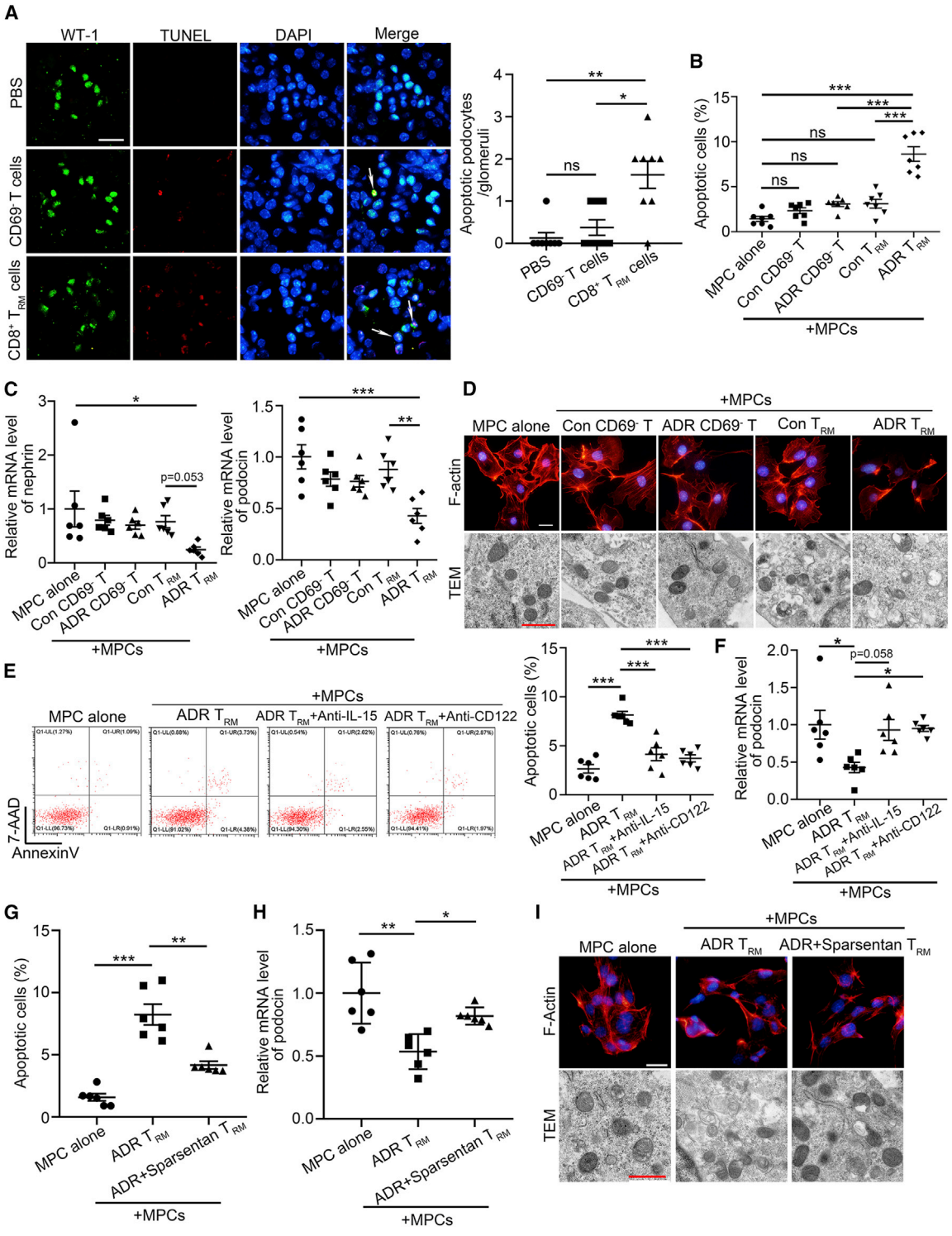

Figure 7. Activated renal CD8$^+$ T_{RM} cells trigger podocyte injury

See also Figure S6. (A) Representative immunofluorescence images and quantifications of apoptotic podocytes per glomeruli by TUNEL assay (10 areas per mouse were analyzed); white arrows highlight the apoptotic podocytes. Scale bars: black, 20 μm; red, 1 μm (n = 8). (B) The percentage of apoptotic murine podocytes (MPCs, n = 7). (C) Relative mRNA levels of nephrin and podocin in MPCs (n = 6). (D) Morphological examinations of cytoskeleton and mitochondria injury by F-actin staining and transmission

(legend continued on next page)

T_{RM} cells than other cell types in the kidney. Furthermore, $CD8^+$ T_{RM} cells are mostly accumulated surrounding the glomeruli; how cytotoxic $CD8^+$ T_{RM} cells influence podocytes remains unclear. Normally, podocytes are not accessible to $CD8^+$ T cells. However, under some pathogenetic conditions, such as crescentic glomerulonephritis or the late stage of DKD, breaches in Bowman's capsule can allow access of $CD8^+$ T cells to the glomerular tuft and podocytes, resulting in their destruction.[36] However, the breached Bowman's capsule is not observed in FSGS.[37] Therefore, the implication of periglomerular $CD8^+$ T_{RM} cells in podocyte injury is closely associated with different glomerular diseases or different stage of diseases. In this study, it is possible that IFN-γ produced by $CD8^+$ T_{RM} cells may potentiate robust local expression of chemokines and rapidly recruit other circulating inflammatory immune cells into glomeruli, which could amplify immune responses and result in podocyte injury. On the other hand, based on the results from *in vitro* studies by using a transwell co-culture system, renal $CD8^+$ T_{RM} cells from ADR-treated mice had cytotoxic effects on podocytes. Therefore, it is also possible that $CD8^+$ T_{RM} cells might release inflammatory cytokines, which get into glomeruli to injure podocytes directly. Of course, we cannot exclude that under some certain pathogenetic conditions, breaches in Bowman's capsule allow access of $CD8^+$ T_{RM} cells to the glomerular tuft and podocytes, resulting in podocyte injury. Therefore, further studies for addressing this issue are also of great interest.

In conclusion, our studies for the first time provide direct evidence for the pivotal role of renal $CD8^+$ T_{RM} cells, suggesting that targeting T_{RM} cells may represent a novel therapeutic strategy for patients with glomerular diseases.

MATERIALS AND METHODS

Human renal biopsy samples

Renal biopsies had been performed as part of routine clinical diagnostic investigation. The samples of renal biopsies were obtained from Department of Pathology, Shandong University School of Basic Medical Sciences. Normal controls were obtained from the healthy kidney poles of individuals who underwent tumor nephrectomies without other kidney diseases. The investigations were conducted in accordance with the principles of the Declaration of Helsinki and were approved by the Research Ethics Committee of Shandong University after informed consent was obtained from the patients.

Animal studies

All experimental protocols for animal studies were approved by the Institutional Animal Care and Use Committee of the School of Basic Medical Sciences, Shandong University (document no. ECSBM SSDU2018-2-074) and conducted in accordance with the National Institutes of Health *Guide for the Care and Use of Laboratory Animals*. Different groups were allocated in a randomized manner and investigators were blinded to the allocation of different groups when doing surgeries and doing outcome evaluations. The mouse models used in this study were described in the supplemental methods.

Cells isolation and sorting

The kidney was enzymatically digested with 400 μg/mL collagenase D (Roche, Mannheim, Germany) and 10 U/mL DNase I (Roche, Mannheim, Germany) for 45 min at 37°C. Subsequently, leukocytes were isolated by density gradient centrifugation using 40% Percoll (Merck Millipore, Darmstadt, Germany). $CD8^+CD69^-CD44^+$ T cells or renal $CD8^+$ T_{RM} cells were purified with fluorescence-activated cell sorting (MoFlo Astrios EQ, Beckman Coulter).

Adoptive transfer

Splenic $CD8^+CD69^-CD44^+$ cells were adoptively transferred to nude mice by a single tail-vein injection (106/head). Renal $CD8^+$ $CD69^-CD44^+$ T cells, and $CD8^+$ T_{RM} cells from ADR-treated mice were adoptively transferred to nude mice by a single tail-vein injection (106/head).

In vivo labeling assay

Intravascular injection of anti-CD45 mAb (clone: 30-F11, 2.5 μg per mouse) was administered to mice 5 min before sacrifice.[38,39]

Mass cytometry

The detailed methods are described in the supplemental method. A summary of the antibodies/clones used in the mass cytometry analysis is presented in the Tables S1 and S2.

Flow cytometry

Surface IF staining was performed at 4°C for 30 min. For intracellular (IC) cytokine staining, cells were stimulated with 50 ng/mL phorbol-12-myristate-13-acetate (PMA, MultiSciences), 1 μg/mL ionomycin (MultiSciences), and brefeldin A (5 μg/mL) for 5 h. Cells were fixed with IC fixation buffer (Invitrogen) after surface staining, permeabilized with permeabilization buffer (Invitrogen), and stained with IC antibodies cocktail for 30 min at 4°C. A summary of the antibodies/clones used in the flow cytometry analysis is presented in the Table S3. Cells were then washed and resuspended in phosphate buffer saline. Acquisition was performed on a CytoFLEX S Flow Cytometer, and data were analyzed using CytExpert software (both from Beckman Coulter).

Cell culture

The detailed cell preparations and cell culture conditions of murine podocyte cell line (MPC), glomerular mesangial cell line (MC), and

electron microscopy (TEM) analyses in MPCs. Scale bars: black, 20 μm; red, 1 μm. (E) Representative flow cytometric analyze and quantification of apoptotic MPCs (n = 6). (F) Relative mRNA levels of podocin in MPCs (n = 6). (G) The percentage of apoptotic MPCs (n = 6).
(H) Relative mRNA levels of podocin in MPCs (n = 6). (I) Morphological examinations of cytoskeleton and mitochondria injury by F-actin staining and TEM analyses in MPCs. Scale bars: black, 20 μm; red, 1 μm. Data are represented as mean ± SEM. *p < 0.05, **p < 0.01, ***p < 0.001.

glomerular endothelial cell line (GENC) were briefly described in the supplemental methods.

Transwell migration assay

In a transwell co-culture system, MPCs, MCs, or GENCs (5×10^4, lower) were seeded on a 0.8 mm Transwell insert (Corning, Corning, NY, USA) with medium and co-cultured with renal $CD8^+$ memory T cells (5×10^3, upper) from normal or ADR-treated mice.

Enzyme-linked immunoabsorbent assay

According to the manufacturer's instructions, renal cortex homogenates or cells supernatant samples were analyzed by mouse IL-15 (MultiSciences), ET-1 (OmnimAbs, CA, USA), and Ang II (Omni mAbs, CA, USA) ELISA kit.

Antibody and drug treatment

Anti-mouse IL-15 antibody (300 μg/head; Bio X Cell, clone AIO.3), anti-mouse CD122 antibody (100 μg/head; Bio X Cell, clone TM-beta 1), anti-mouse NK1.1 antibody (200 μg/head; BioLegend, clone PK136), or isotype controls (Bio X Cell, clone C1.18.4) were administered intraperitoneally three times weekly. The current concentrations of IL-15,[40] CD122,[16] and NK1.1[40] neutralizing antibodies were used, as previous studies indicated. Sparsentan (30 μmol/kg, MCE) was administered orally three times weekly. FTY720 (240 μg/kg, MCE) was administered intraperitoneally before ADR treatment.

Transmission electron microscopy

Electron microscopic sample handling and detection were performed by the electron microscopic core lab of Shandong University. Tissues and cells were collected and fixed with 2.5% glutaraldehyde at 4°C. Sections were washed 15 min for 3 times in 0.1 mol/L PBS and post-fixed in 1% osmium tetroxide at room temperature for 2 h. Specimens were then dehydrated using 30%, 50%, 70%, 80%, 90%, 95%, and 100% ethanol and 100% acetone in series. After dehydration, the sections were embedded in Pon 812 resin overnight at 37°C using acetone as a transitional solvent. The ultra-thin sections were cut and post-stained with 2% saturated uranyl acetate and lead citrate.

Multiplex immunohistochemistry staining

The detailed multiplex immunohistochemistry stain method descriptions are available in the supplemental methods. Details of antibodies are described in Table S4.

Immunofluorescence staining

Tissues were transferred to 4% paraformaldehyde (PFA) and fixed at 4°C overnight, followed by paraffin embedded and cross-sectioned (3 μm) for IF staining by using a modified protocol, as previously described.[41] Details of antibodies are described in Table S4.

TUNEL assay

Cell death in the kidney section was detected by TUNEL assay following the manufacturer's protocol (Roche Diagnostics, Mannheim, Germany).

RNA extraction and real-time quantitative PCR

Total RNA was isolated from cells using TRIzol reagent (Invitrogen). The mRNA expression levels were determined by real-time quantitative RT-PCR using a Bio-Rad iCycler system (Bio-Rad, Hercules, CA). The sequences of specific primers are listed in Table S5.

Statistics

Data are expressed as mean ± SEM. Statistical analyses were performed with GraphPad Prism (v.8.0, GraphPad Software, San Diego, CA). Normality assumption of the data distribution was assessed using Kolmogorov-Smirnov test. Comparisons between two groups were performed using two-tailed Student's t test for normally distributed data and Mann-Whitney rank-sum test for non-normally distributed data. Differences between multiple groups with one variable were determined using one-way ANOVA followed by *post hoc* Tukey's test. To compare multiple groups with more than one variable, two-way ANOVA followed by *post hoc* Tukey's test was used. For correlation analysis, Pearson correlation coefficient was applied as appropriate.

SUPPLEMENTAL INFORMATION

Supplemental information can be found online at https://doi.org/10.1016/j.ymthe.2022.04.024.

ACKNOWLEDGMENTS

We thank Translational Medicine Core Facility of Shandong University for consultation and instrument availability that supported this work. This study was supported by the National Nature Science Foundation of China (91949202, 82090020, 82090024, 81970580, 81800645, 81800643, 81873614, and 81900659); National Key R&D Program of China (2020YFC2005000); and Shandong Provincial Natural Science Foundation, China (ZR2019ZD40 and ZR2019BH030).

AUTHOR CONTRIBUTIONS

L.L., W.T., Y.Z., and M.J. conducted experiments, performed data analysis, and helped write the manuscript. L.W. helped analyze flow cytometry data. Q.L., Q.H., and X.P. contributed with cells isolation from animals. Y.Z. and J.W. performed *in vivo* animal studies. W.T. and Y.X. helped design experiments. Z.W., J.Z., X.W., M.L., Y.S., and C.Z. analyzed human renal biopsy samples. F.Y. designed the experiment, interpreted the data, wrote the manuscript, and approved the final version of the manuscript for publication.

DECLARATION OF INTERESTS

All authors declare no conflict of interest.

REFERENCES

1. Schenkel, J.M., and Masopust, D. (2014). Tissue-resident memory T cells. Immunity *41*, 886–897. https://doi.org/10.1016/j.immuni.2014.12.007.

2. Mueller, S.N., and Mackay, L.K. (2016). Tissue-resident memory T cells: local specialists in immune defence. Nat. Rev. Immunol. *16*, 79–89. https://doi.org/10.1038/nri.2015.3.

3. Mueller, S.N., Gebhardt, T., Carbone, F.R., and Heath, W.R. (2013). Memory T cell subsets, migration patterns, and tissue residence. Annu. Rev. Immunol. *31*, 137–161. https://doi.org/10.1146/annurev-immunol-032712-095954.

4. Takamura, S. (2018). Niches for the long-term maintenance of tissue-resident memory T cells. Front. Immunol. *9*, 1214. https://doi.org/10.3389/fimmu.2018.01214.

5. Shin, H. (2018). Formation and function of tissue-resident memory T cells during viral infection. Curr. Opin. Virol. *28*, 61–67. https://doi.org/10.1016/j.coviro.2017.11.001.

6. Shin, H., and Iwasaki, A. (2013). Tissue-resident memory T cells. Immunol. Rev. *255*, 165–181. https://doi.org/10.1111/imr.12087.

7. Krebs, C.F., Reimers, D., Zhao, Y., Paust, H.J., Bartsch, P., Nunez, S., Rosemblatt, M.V., Hellmig, M., Kilian, C., Borchers, A., et al. (2020). Pathogen-induced tissue-resident memory TH17 (TRM17) cells amplify autoimmune kidney disease. Sci. Immunol. *5*, eaba4163. https://doi.org/10.1126/sciimmunol.aba4163.

8. Nagata, M. (2016). Podocyte injury and its consequences. Kidney. Int. *89*, 1221–1230. https://doi.org/10.1016/j.kint.2016.01.012.

9. Bhargava, R., and Tsokos, G.C. (2019). The immune podocyte. Curr. Opin. Rheumatol. *31*, 167–174. https://doi.org/10.1097/bor.0000000000000578.

10. Li, S., Liu, Y., He, Y., Rong, W., Zhang, M., Li, L., Liu, Z., and Zen, K. (2020). Podocytes present antigen to activate specific T cell immune responses in inflammatory renal disease. J. Pathol. *252*, 165–177. https://doi.org/10.1002/path.5508.

11. Cibrian, D., and Sanchez-Madrid, F. (2017). CD69: from activation marker to metabolic gatekeeper. Eur. J. Immunol. *47*, 946–953. https://doi.org/10.1002/eji.201646837.

12. Zhou, M., Guo, C., Li, X., Huang, Y., Li, M., Zhang, T., Zhao, S., Wang, S., Zhang, H., and Yang, N. (2020). JAK/STAT signaling controls the fate of CD8(+)CD103(+) tissue-resident memory T cell in lupus nephritis. J. Autoimmun. *109*, 102424. https://doi.org/10.1016/j.jaut.2020.102424.

13. Wilk, M.M., Misiak, A., McManus, R.M., Allen, A.C., Lynch, M.A., and Mills, K.H.G. (2017). Lung CD4 tissue-resident memory T cells mediate adaptive immunity induced by previous infection of mice with bordetella pertussis. J. Immunol. *199*, 233–243. https://doi.org/10.4049/jimmunol.1602051.

14. Mackay, L.K., Wynne-Jones, E., Freestone, D., Pellicci, D.G., Mielke, L.A., Newman, D.M., Braun, A., Masson, F., Kallies, A., Belz, G., and Carbone, F. (2015). T-box transcription factors combine with the cytokines TGF-beta and IL-15 to control tissue-resident memory T cell fate. Immunity *43*, 1101–1111. https://doi.org/10.1016/j.immuni.2015.11.008.

15. Ikemizu, S., Chirifu, M., and Davis, S.J. (2012). IL-2 and IL-15 signaling complexes: different but the same. Nat. Immunol. *13*, 1141–1142. https://doi.org/10.1038/ni.2472.

16. Richmond, J.M., Strassner, J.P., Zapata, L., Jr., Garg, M., Riding, R.L., Refat, M.A., Fan, X., Azzolino, V., Tovar-Garza, A., Tsurushita, N., et al. (2018). Antibody blockade of IL-15 signaling has the potential to durably reverse vitiligo. Sci. Transl. Med. *10*, eaam7710. https://doi.org/10.1126/scitranslmed.aam7710.

17. Wang, X., and Zhao, X.Y. (2021). Transcription factors associated with IL-15 cytokine signaling during NK cell development. Front. Immunol. *12*, 610789. https://doi.org/10.3389/fimmu.2021.610789.

18. Davenport, A.P., Kuc, R.E., Southan, C., and Maguire, J.J. (2018). New drugs and emerging therapeutic targets in the endothelin signaling pathway and prospects for personalized precision medicine. Physiol. Res. *67*, S37–S54. https://doi.org/10.33549/physiolres.933872.

19. Komers, R., Gipson, D.S., Nelson, P., Adler, S., Srivastava, T., Derebail, V.K., Meyers, K.E., Pergola, P., MacNally, M.E., Hunt, J.L., et al. (2017). Efficacy and safety of Sparsentan compared with Irbesartan in patients with primary focal segmental glomerulosclerosis: randomized, controlled trial design (DUET). Kidney. Int. Rep. *2*, 654–664. https://doi.org/10.1016/j.ekir.2017.02.019.

20. Tang, S.C., Leung, J.C., Chan, L.Y., Eddy, A.A., and Lai, K.N. (2008). Angiotensin converting enzyme inhibitor but not angiotensin receptor blockade or statin ameliorates murine adriamycin nephropathy. Kidney. Int. *73*, 288–299. https://doi.org/10.1038/sj.ki.5002674.

21. Turner, J.E., Becker, M., Mittrucker, H.W., and Panzer, U. (2018). Tissue-resident lymphocytes in the kidney. J. Am. Soc. Nephrol. *29*, 389–399. https://doi.org/10.1681/asn.2017060599.

22. Wu, H., Liao, W., Li, Q., Long, H., Yin, H., Zhao, M., Chan, V., Lau, C.S., and Lu, Q. (2018). Pathogenic role of tissue-resident memory T cells in autoimmune diseases. Autoimmun. Rev. *17*, 906–911. https://doi.org/10.1016/j.autrev.2018.03.014.

23. Dumauthioz, N., Labiano, S., and Romero, P. (2018). Tumor resident memory T cells: new players in immune surveillance and therapy. Front Immunol. *9*, 2076. https://doi.org/10.3389/fimmu.2018.02076.

24. Milner, J.J., Toma, C., He, Z., Kurd, N.S., Nguyen, Q.P., McDonald, B., Quezada, L., Widjaja, C.E., Witherden, D.A., Crowl, J.T., et al. (2020). Heterogenous populations of tissue-resident CD8(+) T cells are generated in response to infection and malignancy. Immunity *52*, 808–824.e7. https://doi.org/10.1016/j.immuni.2020.04.007.

25. Yang, K., and Kallies, A. (2021). Tissue-specific differentiation of CD8(+) resident memory T cells. Trends. Immunol. *42*, 876–890. https://doi.org/10.1016/j.it.2021.08.002.

26. Patidar, M., Yadav, N., and Dalai, S.K. (2016). Interleukin 15: a key cytokine for immunotherapy. Cytokine Growth Factor Rev. *31*, 49–59. https://doi.org/10.1016/j.cytogfr.2016.06.001.

27. Adachi, T., Kobayashi, T., Sugihara, E., Yamada, T., Ikuta, K., Pittaluga, S., Saya, H., Amagai, M., and Nagao, K. (2015). Hair follicle-derived IL-7 and IL-15 mediate skin-resident memory T cell homeostasis and lymphoma. Nat. Med. *21*, 1272–1279. https://doi.org/10.1038/nm.3962.

28. Zheng, G., Zheng, L., Wang, Y., Wu, H., Kairaitis, L., Zhang, C., Tay, Y.C., Alexander, S., and Harris, D. (2006). NK cells do not mediate renal injury in murine adriamycin nephropathy. Kidney Int. *69*, 1159–1165. https://doi.org/10.1038/sj.ki.5000244.

29. Campbell, K.N., and Tumlin, J.A. (2018). Protecting podocytes: a key target for therapy of focal segmental glomerulosclerosis. Am. J. Nephrol. *47*, 14–29. https://doi.org/10.1159/000481634.

30. Barton, M., and Sorokin, A. (2015). Endothelin and the glomerulus in chronic kidney disease. Semin. Nephrol. *35*, 156–167. https://doi.org/10.1016/j.semnephrol.2015.02.005.

31. Barton, M. (2011). Endothelin antagonism and reversal of proteinuric renal disease in humans. Contrib. Nephrol. *172*, 210–222. https://doi.org/10.1159/000328702.

32. Komers, R., and Plotkin, H. (2016). Dual inhibition of renin-angiotensin-aldosterone system and endothelin-1 in treatment of chronic kidney disease. Am. J. Physiol. Regul. Integr. Comp. Physiol. *310*, R877–R884. https://doi.org/10.1152/ajpregu.00425.2015.

33. Komers, R., Diva, U., Inrig, J.K., Loewen, A., Trachtman, H., and Rote, W.E. (2020). Study design of the phase 3 sparsentan versus irbesartan (DUPLEX) study in patients with focal segmental glomerulosclerosis. Kidney. Int. Rep. *5*, 494–502. https://doi.org/10.1016/j.ekir.2019.12.017.

34. Crowley, S.D., and Rudemiller, N.P. (2017). Immunologic effects of the renin-angiotensin system. J. Am. Soc. Nephrol. *28*, 1350–1361. https://doi.org/10.1681/asn.2016101066.

35. Khan, T.N., Mooster, J.L., Kilgore, A.M., Osborn, J.F., and Nolz, J.C. (2016). Local antigen in nonlymphoid tissue promotes resident memory CD8+ T cell formation during viral infection. J. Exp. Med. *213*, 951–966. https://doi.org/10.1084/jem.20151855.

36. Chen, A., Lee, K., D'Agati, V.D., Wei, C., Fu, J., Guan, T.J., He, J.C., Schlondorff, D., and Agudo, J. (2018). Bowman's capsule provides a protective niche for podocytes from cytotoxic CD8+ T cells. J. Clin. Invest. *128*, 3413–3424. https://doi.org/10.1172/jci97879.

37. Kuppe, C., Grone, H.J., Ostendorf, T., van Kuppevelt, T.H., Boor, P., Floege, J., Smeets, B., and Moeller, M.J. (2015). Common histological patterns in glomerular epithelial cells in secondary focal segmental glomerulosclerosis. Kidney. Int. *88*, 990–998. https://doi.org/10.1038/ki.2015.116.

38. Anderson, K.G., Sung, H., Skon, C.N., Lefrancois, L., Deisinger, A., Vezys, V., and Masopust, D. (2012). Cutting edge: intravascular staining redefines lung CD8 T cell responses. J. Immunol. *189*, 2702–2706. https://doi.org/10.4049/jimmunol.1201682.

39. Anderson, K.G., Mayer-Barber, K., Sung, H., Beura, L., James, B.R., Taylor, J.J., Qunaj, L., Griffith, T.S., Vezys, V., Barber, D.L., and Masopust, D. (2014). Intravascular staining for discrimination of vascular and tissue leukocytes. Nat. Protoc. *9*, 209–222. https://doi.org/10.1038/nprot.2014.005.

40. Koda, Y., Teratani, T., Chu, P.S., Hagihara, Y., Mikami, Y., Harada, Y., Tsujikawa, H., Miyamoto, K., Suzuki, T., Taniki, N., et al. (2021). CD8(+) tissue-resident memory T cells promote liver fibrosis resolution by inducing apoptosis of hepatic stellate cells. Nat. Commun. *12*, 4474. https://doi.org/10.1038/s41467-021-24734-0.

41. Fu, Y., Sun, Y., Wang, M., Hou, Y., Huang, W., Zhou, D., Wang, Z., Yang, S., Tang, W., Zhen, J., et al. (2020). Elevation of JAML promotes diabetic kidney disease by modulating podocyte lipid metabolism. Cell. Metab. *32*, 1052–1062.e8. https://doi.org/10.1016/j.cmet.2020.10.019.

YMTHE, Volume *30*

Supplemental Information

Targeting tissue-resident memory $CD8^+$ T cells in the kidney is a potential therapeutic strategy to ameliorate podocyte injury and glomerulosclerosis

Liang Li, Wei Tang, Yan Zhang, Meng Jia, Limei Wang, Quanxin Li, Qingsheng Han, Xiuping Peng, Yusheng Xie, Jichao Wu, Ziying Wang, Junhui Zhen, Xiaojie Wang, Min Liu, Yu Sun, Chun Zhang, and Fan Yi

Supplemental Figures

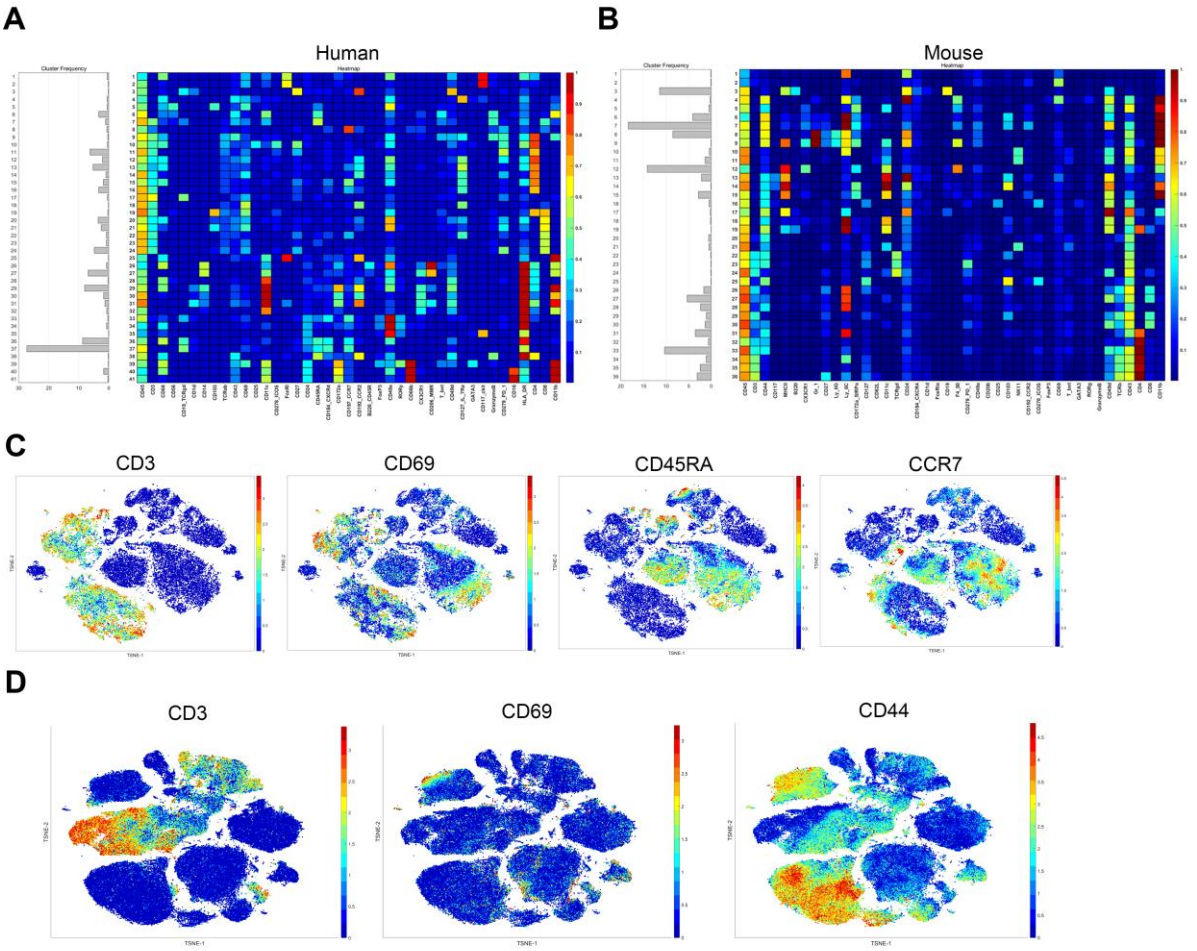

Figure S1. The immune landscape of human and mouse kidney. (A-B) Heat-plot summary of average median expression of each cellular marker analyze in human (A) and mouse (B) kidney. (C) t-distributed stochastic neighbor embedding (TSNE) analysis of immune cells from normal human kidney colored by relative expression of CD3, CD69, CD45RA, CCR7. (D) TSNE analysis of immune cells from normal mouse kidney colored by relative expression of CD3, CD69, CD44.

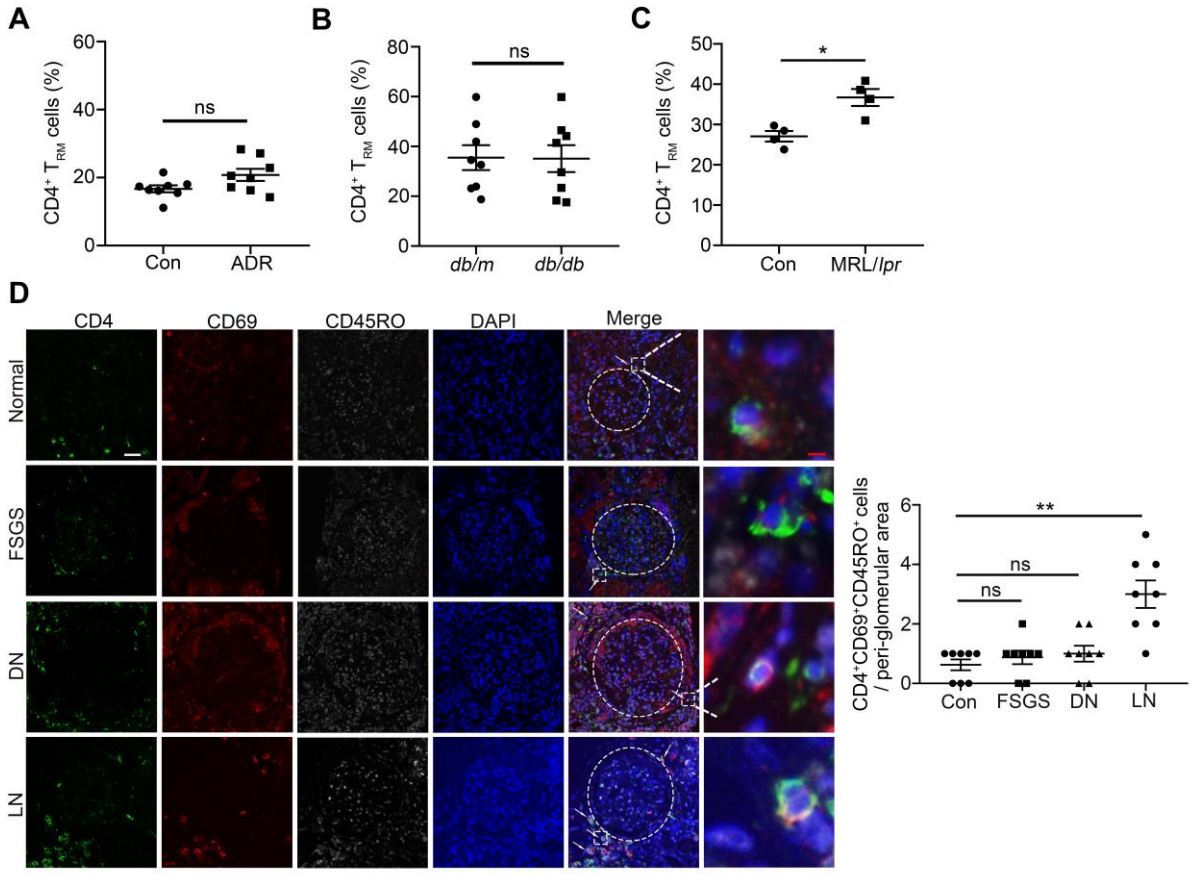

Figure S2: The proportion of CD4$^+$ T$_{RM}$ cells in mice and patients with glomerular disease: (A-C) Quantification of renal CD4$^+$ T$_{RM}$ (CD4$^+$CD69$^+$CD44$^+$) cells in ADR-treated mice (A, n = 8), *db/db* mice (B, n = 8), MRL/*lpr* mice (C, n = 4) and their controls. (D) Representative immunofluorescence staining for CD4 (green), CD69 (red), CD45RO (gray) in human renal tissues from normal, subjects with FSGS, DN and LN. Left: representative images, white arrows highlight CD4$^+$ T$_{RM}$ cells (CD4$^+$CD69$^+$CD45RO$^+$), scale bar: white 70 μm, red 5 μm; right: quantification of CD4$^+$ T$_{RM}$ cells surrounding the glomeruli per HPF (n = 8). Data are represented as mean ± SEM. *p<0.05, **p<0.01, ns, no significance.

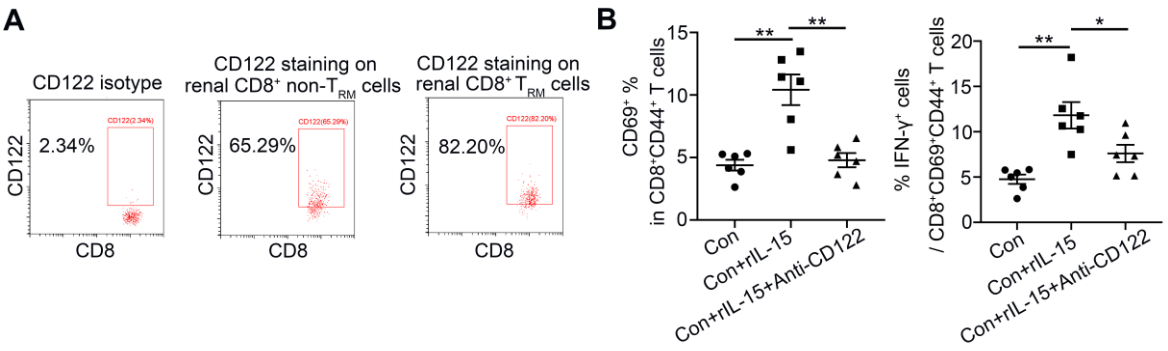

Figure S3. CD122 blockade inhibits CD8$^+$ T_{RM} cell formation and activation *in vitro*. (A) Representative flow cytometry staining of CD122 on renal CD8$^+$ non-T_{RM} and T_{RM} cells. (B) The percentage of CD69$^+$ in splenic CD8$^+$CD44$^+$ T cells and the frequency of IFN-γ in splenic CD8$^+$CD69$^+$CD44$^+$ T cells (n = 6). Data are represented as mean ± SEM. *p<0.05, **p<0.01.

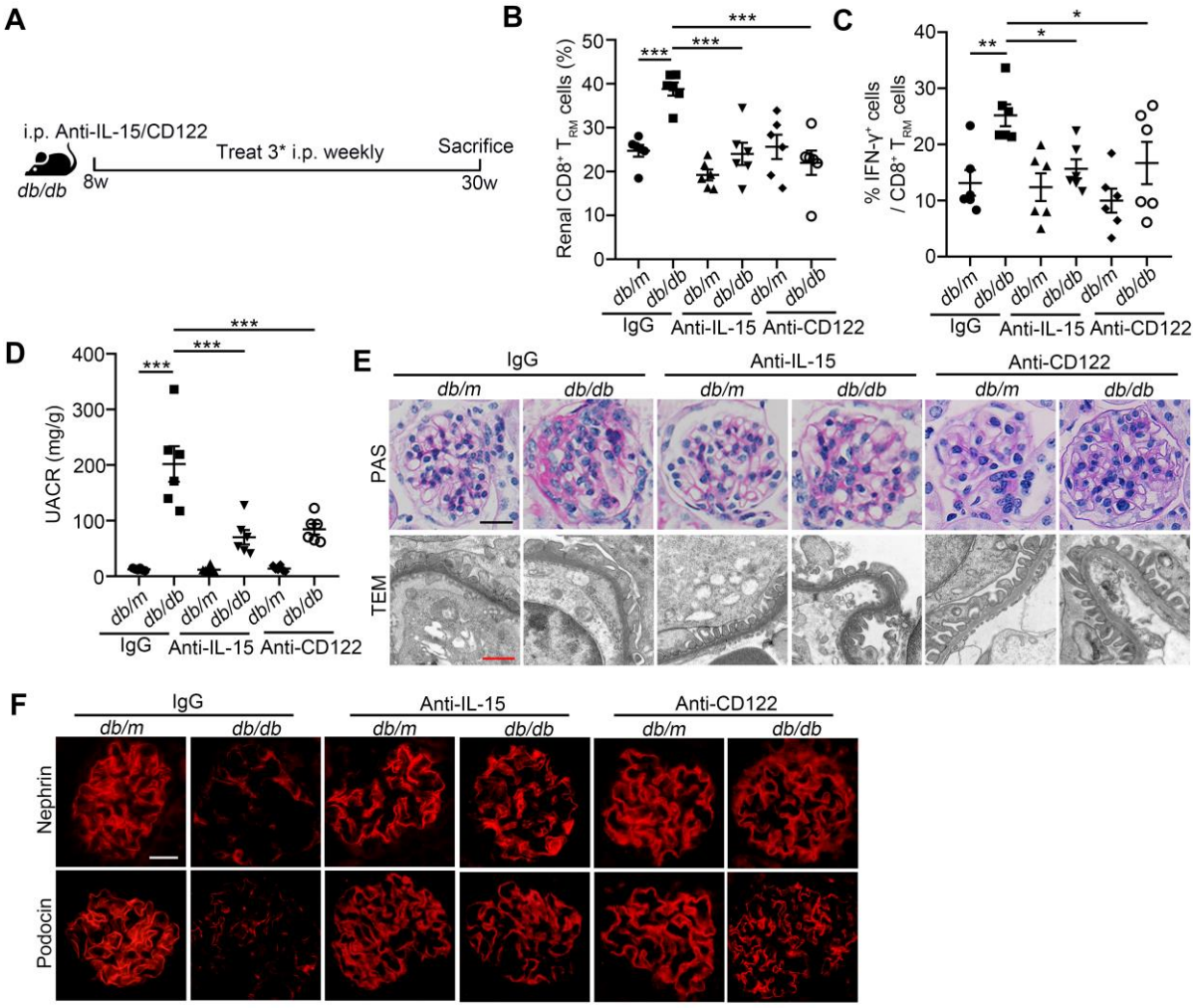

Figure S4: IL-15 signaling blockade reverses glomerulosclerosis and podocyte injury by inhibiting renal CD8$^+$ T$_{RM}$ cells formation and activation in *db/db* mice: (A) A schematic diagram showing the treatment of Anti-IL-15/CD122 in *db/db* mice. (B) The percentage of renal CD8$^+$ T$_{RM}$ cells (n = 6). (C) The frequency of IFN-γ in renal CD8$^+$ T$_{RM}$ cells (n = 6). (D) Urine albumin-to-creatinine ratio (UACR) in mice (n = 6). (E) Morphological examinations of glomerular changes by Periodic acid–Schiff (PAS) and transmission electron microscopy (TEM) analyses in mice. Scale bar: black 20 μm, red 1 μm. (F) Representative IF images about nephrin and podocin expressions in glomeruli from mice. Scale bar, 20 μm. Data are represented as mean ± SEM. *p<0.05, **p<0.01, ***p<0.001.

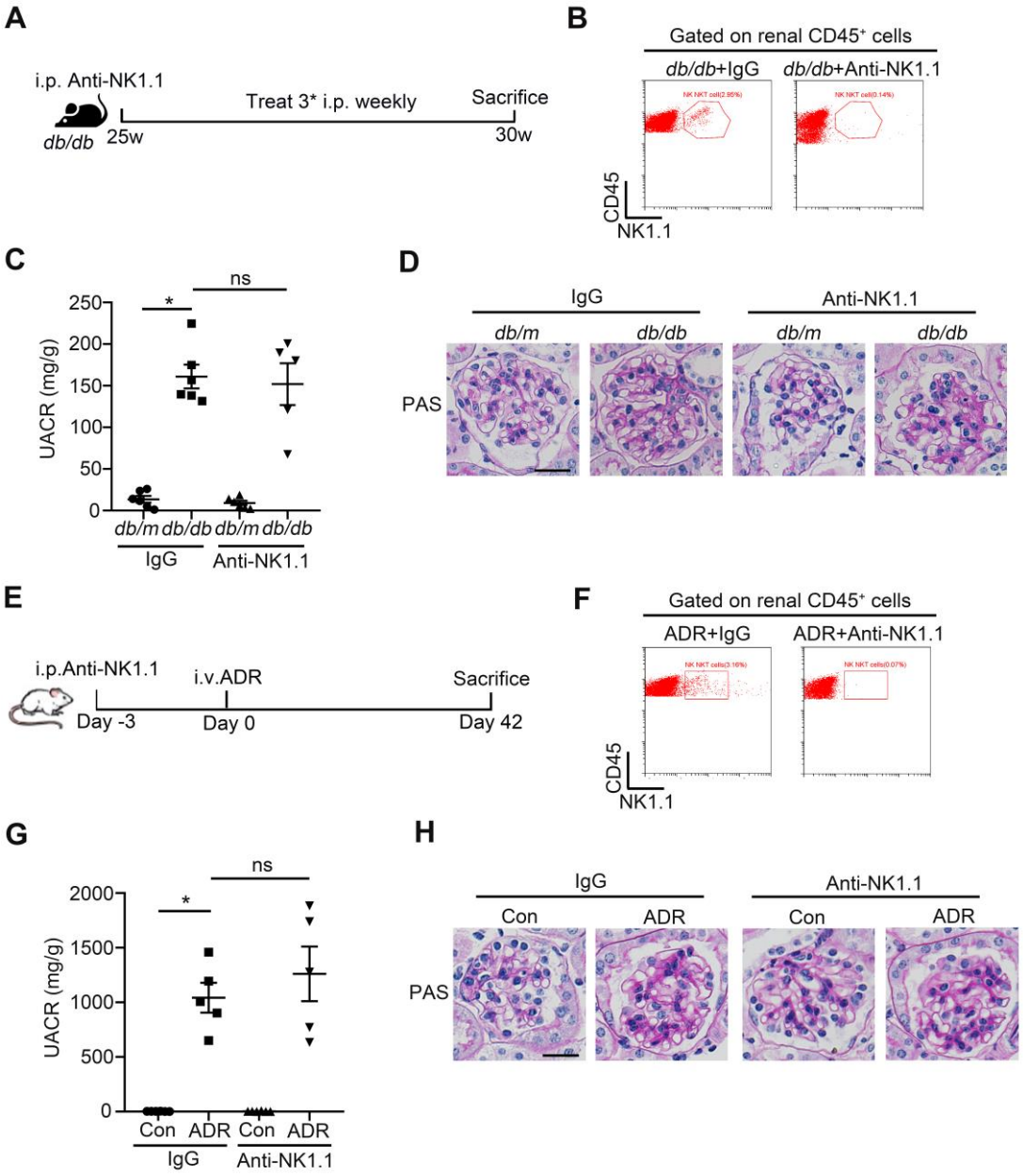

Figure S5 NK cell cannot mediate glomerular injury in *db/db* and ADR-induced mice. (A) A schematic diagram showing the treatment of anti-NK1.1 antibody in *db/db* mice. (B) Representative flow cytometry staining of NK1.1 on renal CD45$^+$ cells in *db/db* mice. (C) Urine albumin-to-creatinine ratio (UACR) in *db/db* mice with the treatment of anti-NK1.1 (n = 6). (D) Morphological examinations of glomerular changes in *db/db* mice with the treatment of anti-NK1.1. Scale bar, 20 μm. (E) A schematic diagram showing the treatment of anti-NK1.1 antibody in ADR-treated mice. (F) Representative flow cytometry staining of NK1.1 on renal CD45$^+$ cells in ADR-treated mice. (G) UACR in ADR-treated mice with the treatment of anti-NK1.1 (n = 5). (H) Morphological examinations of glomerular changes in ADR-treated mice with the treatment of anti-NK1.1. Scale bar, 20 μm. Data are represented as mean ± SEM. *p<0.05, ns, no significance.

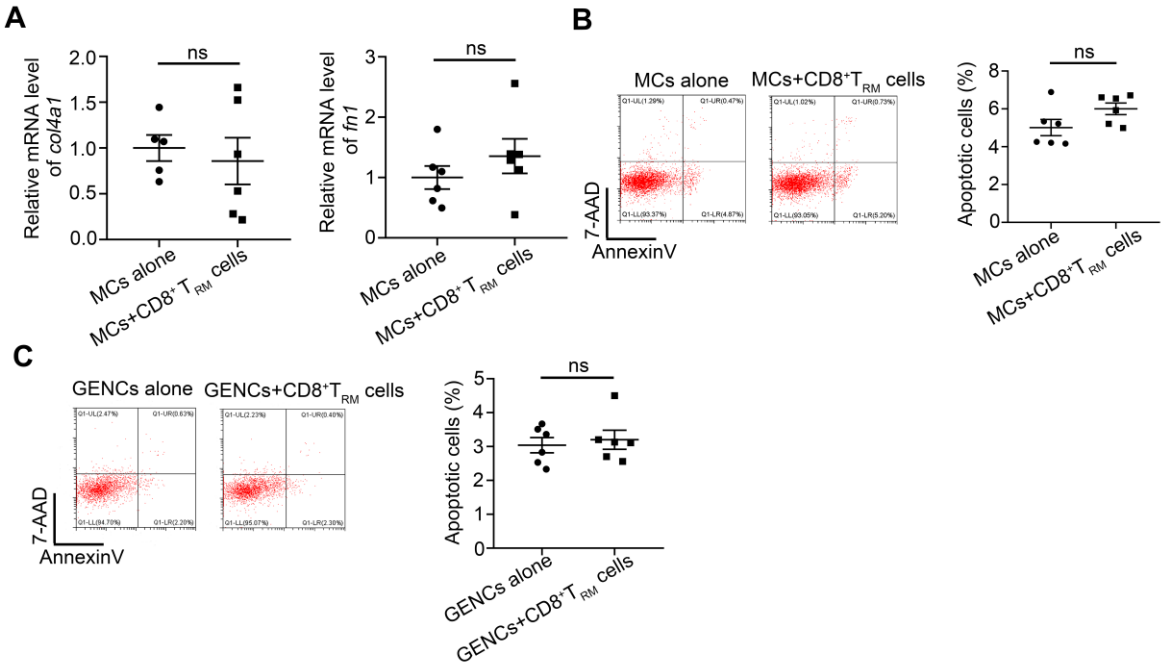

Figure S6 Renal activated CD8$^+$ T_{RM} cells have no impact on glomerular mesangial cells and endothelial cells. (A) Relative mRNA levels of *col4a1* and *fn1* in murine glomerular mesangial cells (MCs, n = 6). (B) Representative flow cytometric analyze and quantification of apoptotic murine MCs (n = 6). (C) Representative flow cytometric analyze and quantification of apoptotic murine glomerular endothelial cells (GENCs, n = 6). Data are represented as mean ± SEM. ns, no significance.

Supplemental Tables

Table S1. The list of antibodies used for mass cytometry analysis in human kidney

Parameter	Metal	Clone	Producer
CD45	89Y	HI30	BioLegend
CD3	115In	UCHT1	BioXcell
CD68	139La	Y1/82A	BioLegend
CD56	141Pr	NCAM16.2	BD
TCRγδ	142Nd	5A6.E9	Homemade
CD19	142Nd	HIB19	BioLegend
CD1d	143Nd	51.1	BioLegend
CD14	144Nd	M5E2	BioLegend
CD103	145Nd	B-Ly7	eBioscience
TCRαβ	146Nd	AER-37[CRA-1]	BioLegend
CD43	147Sm	O323	eBioscience
CD69	148Nd	ML5	BioLegend
CD25	149Sm	HI100	R&D
CD11c	150Nd	12G5	BioLegend
CD278[ICOS]	151Eu	SE5A5	BioLegend
FceRIα	152Sm	G043H7	BioLegend
CD27	153Eu	K036C2	BioLegend
CD24	154Sm	RA3-6B2	BioLegend
CD45RA	155Gd	PCH101	BioLegend
CD184[CXCR4]	156Gd	TS2/7	BioLegend
CD172a	157Gd	600214	BioLegend
CD197[CCR7]	158Gd	G10F5	BioLegend
CD192[CCR2]	159Tb	K0124E1	BioLegend
B220[CD45R]	160Gd	15-2	BioLegend
FoxP3	162Dy	4B10	eBioscience

CD49a	163Dy	9F10	BioLegend
RORγ	164Dy	A019D5	R&D
CD66b	165Ho	TWAJ	BioLegend
CX3CR1	166Er	104D2	BioLegend
CD206	167Er	GB11	BioLegend
T-bet	168Er	EH12.2H7	BioLegend
CD49d	169Tm	3G8	BioLegend
CD127[IL-7Rα]	170Er	L243	BioLegend
GATA3	171Yb	RPA-T4	eBioscience
CD117	172Yb	RPA-T8	BioLegend
Granzyme B	173Yb	M1/70	Fluidigm
CD279[PD-1]	174Yb	AER-37[CRA-1]	BioLegend
CD16	175Lu	O323	BioLegend
HLA-DR	176Yb	ML5	BioLegend
CD4	197Au	HI100	BioLegend
CD8	198Pt	12G5	BioLegend
CD11b	209Bi	SE5A5	BioLegend

Table S2. The list of antibodies used for mass cytometry analysis in mouse kidney

Parameter	Metal	Clone	Producer
CD45	89Y	30-F11	BioLegend
CD3	115In	145-2C11	BioLegend
CD44	139La	IM7	BioLegend
CD117	141Pr	2B8	BioLegend
MHC II	142Nd	M5/114.15.2	BioLegend
B220	143Nd	RA3-6B2	BioLegend
CX3CR1	144Nd	SA011F11	BioLegend
Gr1	145Nd	RB6-8C5	BioLegend
CD27	146Nd	LG.3A10	BioLegend
Ly6G	147Sm	1A8	BioLegend
Ly6C	148Nd	HK1.4	BioLegend
CD172a	149Sm	P84	BioLegend
CD127	150Nd	A7R34	BioLegend
CD62L	151Eu	MEL14	BioLegend
CD11c	152Sm	N418	BioLegend
TCRγδ	153Eu	GL3	BioLegend
CD24	154Sm	M1/69	BioLegend
CD184[CXCR4]	155Gd	L276F12	BioLegend
CD1d	156Gd	1B1	BioLegend
FceRIα	157Gd	MAR-1	BioLegend
CD19	158Gd	6D5	BioLegend
F4/80	159Tb	C1:A3-1	BioRad
CD279[PD-1]	160Gd	29F.1A12	BioLegend
CD49a	161Dy	HMa1	BioLegend

CD206	162Dy	C068C2	BioLegend
CD25	163Dy	3C7	BioLegend
CD103	164Dy	2E7	BioLegend
NK1.1	165Ho	PK136	BioLegend
CD192[CCR2]	166Er	SA044G4	BioLegend
CD278[ICOS]	167Er	C398.4A	BioLegend
FoxP3	168Er	FJK-16s	eBioscience
CD69	169Tm	H1.2F3	BioLegend
T-bet	170Er	4B10	BioLegend
GATA3	171Yb	TWAJ	eBioscience
RORγ	172Yb	600214	R&D
Granzyme B	173Yb	GB11	Fluidigm
CD49d	174Yb	R1-2	BioLegend
TCRαβ	175Lu	H57-597	BioLegend
CD43	176Yb	S11	BioLegend
CD4	197Au	RM4-5	BioLegend
CD8a	198Pt	53-6.7	BioLegend
CD11b	209Bi	M1/70	BioLegend

Table S3. The list of antibodies used for flow cytometry analysis

Parameter	Host	Producer	Clone	Fluorochrome
CD3	Rat	BioLegend	17A2	FITC
CD3	Rat	BioLegend	17A2	PerCP/Cyanine5.5
CD4	Rat	BioLegend	GK1.5	FITC
CD4	Rat	Biolegend	GK1.5	PE/Cyanine7
CD8a	Mouse	BioLegend	RPA-T8	Brilliant Violet 510™
CD8a	Rat	eBioscience	2.43	PE/Cyanine7
CD69	Armenian Hamster	BioLegend	H1.2F3	PE
CD44	Mouse	BioLegend	BJ18	Pacific Blue™
Fixable Viability Kit		BioLegend		Zombie NIR™
IFN-γ	Rat	BioLegend	XMG1.2	PE/Cyanine7
IFN-γ	Rat	BioLegend	XMG1.2	APC
Perforin	Rat	BioLegend	S16009A	APC
Ki-67	Rat	BioLegend	16A8	FITC
CD62L	Rat	BioLegend	MEL-14	PerCP
CD62L	Rat	BioLegend	MEL-14	Brilliant Violet 510™
CXCR3	Mouse	BioLegend	G025H7	PE/Cyanine7
CD122	Rat	BioLegend	TM-β1	APC
NK1.1	Mouse	BioLegend	PK136	PerCP/Cyanine5.5

Table S4. The list of antibodies used for immunofluorescence staining

Primary Antibodies	Host	Dilution and supplier	Product ID
CD4	Rabbit	1:100; Abcam, Cambridge, MA	Ab133616
CD8	Rabbit	1:100; Abcam, Cambridge, MA	Ab93278
CD69	Rabbit	1:100; Abcam, Cambridge, MA	Ab233396
CD45RO	Mouse	1:100; Cell signaling technology, Danvers, MA	55618
Nephrin	Goat	1:50; R&D Systems, Minneapolis, MN	AF3159
Podocin	Rabbit	1:50; Boster, Wuhan, China	BA1688
WT-1	Rabbit	1:50; ZENBIO, Wuhan, China	380948

Table S5. Primer pairs of target genes used for real time RT-PCR in this study

Gene	Species	Primer sequences
NEPHRIN	Mouse	Forward: AGAACTTGCCACCTGATTCCC Reverse: CCTTCCACCACAGTCAGGTTT
PODOCIN	Mouse	Forward: TCCAGCTTCGATACTTGCACA Reverse: CTCCCTTGTGCTCTGTTGCC
COL4A1	Mouse	Forward: AACAACGTCTGCAACTTCGC Reverse: CTTCACAAACCGCACACCTG
FN1	Mouse	Forward: AGTTTGTGCATGGTGTCCGA Reverse: CAGTTGTGCCTGGGTAGGTC
β-Actin	Mouse	Forward: GGCTGTATTCCCCTCCATCG Reverse: CCAGTTGGTAACAATGCCATGT

Supplemental Methods

Adriamycin (ADR)-induced FSGS in mice: Wild-type BALB/c and BALB/c nude mice (male, 6-8 weeks old) were purchased from Beijing Vital River Laboratory Animal Technology Company (Beijing, China). Male mice were administered ADR (10 mg/kg) intravenously by tail vein injection. Urine was collected weekly to assess for albuminuria, and mice were sacrificed at 6 weeks after treatment. At the end of the study, blood and 24 h urine samples were collected for biochemical testing. Simultaneously, the mice were euthanized and the kidney tissue samples were harvested for histopathological analysis.

Spontaneous type 2 diabetic *db/db* mice: Heterozygote BKS *db/m* mice (BKS.Cg-Dock7^{m} +/+Lepr ^{db}/J, Stock No. 000642) and homozygote BKS *db/db* mice (B6.BKS(D)-Lepr^{db}/J, Stock No.000697) were purchased from Jackson Laboratory in the United States. *db/db* mice also could be obtained by self-crossing of *db/m* mice. They produced identifiable obesity phenotypes at 3-4 weeks of age, with elevated blood glucose at 4-8 weeks. *db/m* mice were used as genetic control. Proteinuria will be observed at age of 8-20 weeks as a marker of successful establishment of type 2 DKD models.

Mouse model of systemic lupus erythematosus: Female MRL/*lpr* mice and their control mice MRL/*Mpj* mice were obtained from SLAC Laboratory Animal Company (Shanghai, China).

Cell Culture: The conditionally immortalized murine podocyte cell line (MPC) was a kind gift from Prof. Pin-Lan Li (Department of Pharmacology, Virginia Commonwealth University, USA) and cultured under growth permissive conditions at 33 ℃ in RPMI 1640 supplemented with 10% fetal bovine serum (FBS), 20 U/mL mouse recombinant interferon-γ (IFN-γ), and 100 U/mL penicillin plus 0.1 mg/mL streptomycin. To induce differentiation, podocytes were maintained in non-permissive conditions at 37 ℃ without IFN-γ for 7 days and used for the experiments. Murine glomerular mesangial cells (MCs) were obtained from American Type Culture Collection (ATCC) and cultured in DMEM containing 1.5 g/L sodium bicarbonate, 4.5 g/L glucose. 0.4 mg/mL G418, 4 mmol/L L-glutamine, 100 U/mL penicillin plus 0.1 mg/mL streptomycin supplemented with 5% FBS. Murine glomerular endothelial cells (GENCs) were obtained from Creative Bioarray (USA) and cultured in Dulbecco's Modified Eagle's Medium (DMEM)/F12 supplemented with 5% FBS and 100 U/mL penicillin plus 0.1 mg/mL streptomycin.

Mass cytometry: All samples were thawed and stained with 100 μL of 250 nM cisplatin (Fluidigm) for 5min on ice to exclude dead cells and then incubated in Fc receptor blocking solution before stained with surface antibodies cocktail for 30 min on ice. Cells were fixed in 200 μL of intercalation solution (Maxpar Fix and Perm Buffer containing 250 nM 191/193Ir, Fluidigm) overnight. After fixation, cells were washed once with FACS buffer and then stained with intracellular antibodies cocktail for 30 min on ice. Finally, cells were resuspended with deionized water, adding into 20% EQ beads (Fluidigm), acquired on a mass cytometer (Helios, Fluidigm). All analyses after preprocessing were performed on inverse hyperbolic sine transformed data.

Multiplex immunohistochemistry staining: Opal 4-colour kit (abs50012, absin) was used for multiplex immunohistochemistry staining. Renal biopsy sections were dewaxed and rehydrated. After antigen retrieval, slides were blocked with goat serum for 1 h. The primary antibody, CD8 or CD4 was incubated at room temperature (RT) for 1 h. Slides were washed and incubated with HRP-conjugated secondary antibody at RT for 10 min. TSA dye520 was applied for 10 min after washed. The second antibody, CD69 was incubated overnight at 4 °C. And then, TSA dye600 was applied. The last antibody, CD45RO was incubated at RT for 1 h, and TSA dye650 was applied. Finally, we used DAPI to highlight all nuclei.